

Water-mass formation and Sverdrup dynamics; a comparison between climatology and a coupled ocean–atmosphere model

Matthew H. England^a, Matthias Tomczak^a and J. Stuart Godfrey^b

^a Department of Geology and Geophysics, F05. The University of Sydney, N.S.W. 2006, Australia

^b CSIRO Division of Oceanography, GPO Box 1538 Hobart, Tasmania 7001, Australia

Received June 25, 1991; revised version accepted December 20, 1991

ABSTRACT

England, M.H., Tomczak, M. and Godfrey, J.S., 1992. Water-mass formation and Sverdrup dynamics; a comparison between climatology and a coupled ocean–atmosphere model. *J. Mar. Syst.*, 3: 279–306.

The coupled ocean–atmosphere model integrations of Manabe and Stouffer (1988) are compared with climatological distributions of depth-integrated flow and water-mass formation. The description of the ocean circulation in their two quasi-stable equilibria is extended to include an analysis of the horizontal and meridional mass transport as well as the water-mass formation and vertical motion in the model. In particular, the wind-driven Sverdrup flow is computed and compared with the actual mass transport streamfunction of the model. It is found that a Sverdrup model of depth-integrated flow captures the major features of the coupled model's ocean circulation, except near regions of deep water formation, where the thermohaline field drives ocean currents and wind-driven flow becomes secondary. The coupled model fails to allow for a barotropic mass transport through the Indonesian Passage. Instead, only baroclinically driven fluxes of heat and freshwater are resolved through the Indonesian Archipelago. The Sverdrup model suggests that a barotropic throughflow would transport about 16 Sv from the Pacific to Indian Oceans. According to Sverdrup dynamics, this would serve to weaken the East Australian Current by about 16 Sv and strengthen the Agulhas Current by the same amount. Recent integrations of a World Ocean model with and without a barotropic throughflow in the Indonesian Passage suggest that the modelled heat transport is sensitive to the nature of flow through the Indonesian Archipelago.

From a comparison of observed and simulated water mass properties, it is shown that some major aspects of the global-scale water masses are not captured by the coupled model. This reveals a shortcoming of the model's ability to represent the global-scale heat and freshwater balances. For example, there is an unrealistically intense halocline in the immediate vicinity of Antarctica, prohibiting the formation of bottom water in the Weddell and Ross Seas. Also, no low salinity traces of Antarctic or North Pacific Intermediate Water appear in the model integrations, primarily because there is no source of sufficiently dense bottom water adjacent to Antarctica. Without this dense bottom water, the “would-be” intermediate water at 60°S sinks to great depths and actually becomes the model ocean's bottom water. Then, the simulated bottom water is too fresh and warm in the climate model, matching the temperature–salinity signature of Antarctic Intermediate Water. In the North Atlantic, whilst deep water formation appears in one of the climate states of Manabe and Stouffer (1988), its downward penetration is not as deep as observed. This is because their deep North Atlantic is not ventilated by the thermohaline overturning of warm salty North Atlantic Deep Water. Instead, a deep overturning cell centred near the equator transports relatively fresh water into the region. In contrast, the location and strength of Central Water formation agrees well with climatology.

Introduction

The circulation of the World Ocean is a major component of the global climate system. Because

the ocean has such a high capacity to store heat, any significant change in the World Ocean circulation will result in changes to the earth's climate. Furthermore, because the ocean is driven by air/sea fluxes of heat, mass and momentum, any changes in the earth's climate will alter ocean circulation. So, the ocean and atmosphere behave as a coupled system, so that the modelling of

Correspondence to: M.H. England, GRGS/CNRS 18 av. E. Belin, 31055, Toulouse, France

climate change depends on an understanding of ocean circulation and air/sea coupling.

This study focuses on aspects of two quasi-stable equilibria obtained in a coupled ocean-atmosphere model developed at the Geophysical Fluid Dynamics Laboratory (GFDL). The GFDL study was part of an ongoing goal to model climate change associated with recent perturbations in the concentration of certain atmospheric gases. Manabe and Stouffer (1988, hereinafter referred to as MS) found that the model could reach two different quasi-steady states, depending on the initial conditions of the integration. The two climate modes obtained in their study form the basis of this research.

The existence of multiple equilibria in ocean models has been the subject of several recent studies (F. Bryan, 1986; Welander, 1986; Marotzke et al., 1988; Maier-Reimer and Mikolajewicz, 1989; Marotzke and Willebrand, 1991). The MS study was the first to report the existence of multiple equilibria in a *coupled* ocean-atmosphere model. One state resembles the World Ocean as we know it, with deep water formation in the North Atlantic. The second state has no deep water formation in the Northern Hemisphere. The existence of at least two stable modes of thermohaline circulation was also suggested by Broecker et al. (1985), based on the long Greenland ice core records and other geological evidence.

The transient response of the global climate to an increase in atmospheric CO₂ concentration has been investigated numerically by several researchers (e.g., Bryan et al., 1982, 1988; Bryan and Spelman, 1985; Manabe and Bryan, 1985; Stouffer et al., 1989; Washington and Meehl, 1989; Manabe et al., 1990, 1991). One interesting feature to appear in some of these studies (e.g., Stouffer et al., 1989; Washington and Meehl, 1989; Manabe et al., 1990, 1991) is that the rate of North Atlantic Deep Water (NADW) formation decreases significantly in experiments with a simulated increase in greenhouse gases. However, it should be noted that there is a strong climate drift even in the control run of Washington and Meehl (1989). Several researchers have also found observational evidence that NADW formation is

weakening in the present day World Ocean (e.g. Brewer et al., 1983; Roemmich and Wunsch, 1984; Folland et al., 1986; Jones et al., 1986; Street-Perrott and Perrott, 1990), relating changes in the large-scale climate to a decrease in production of deep water in the North Atlantic. This observed decrease in NADW formation may well correspond to natural variability in the global thermohaline circulation. For example, Weaver et al. (1991) use a basin wide ocean general circulation model (GCM) to demonstrate how decadal/interdecadal variability of the ocean's thermohaline circulation can be excited under steady forcing. In any case, the MS study is not only relevant for paleoclimatic considerations, it also has implications for today's World climate.

The findings of Stouffer et al. (1989) provide an illustration of the importance of using a reliable ocean GCM to determine CO₂-induced climate change. Their study suggests that the Southern Ocean will be a massive sink for excess heat associated with a warming of the atmosphere in the presence of higher CO₂ concentrations. Besides the high thermal inertia of the Southern Hemisphere (because of its vast ocean coverage), Stouffer et al. find that a deep meridional overturning cell advects surface thermal anomalies into the ocean interior. This cell is characteristic of the circulation in the Southern Ocean in many recent World Ocean models (e.g., Bryan and Lewis, 1979; MS; Semtner and Chervin, 1988; Toggweiler et al., 1989a,b; England, 1992). It is difficult to measure this overturning cell in the Southern Ocean; it would require a massive deployment of current meters in an already poorly surveyed ocean. However, we can examine aspects of water mass formation in the model to verify that the broad-scale thermohaline field adequately represents climatology.

One of the principal goals of the present study is to evaluate the horizontal and vertical mass transport in the integrations of MS. The horizontal mass transport streamfunction is compared with the depth-integrated flow predicted by a Sverdrup model that allows for circulation around islands. The vertical mass transport is evaluated with a view to determining the water-mass formation processes simulated by the model. It is im-

portant that any model used to investigate climate change be able to simulate the largest-scale features of water-mass formation.

The coupled ocean–atmosphere model is briefly discussed in the second section, along with a description of the Sverdrup model used to determine wind-driven depth-integrated flow. The third section describes the Sverdrup estimated circulation and the actual mass transport stream-function in the ocean states of MS. Not surprisingly, a Sverdrup model of depth-integrated flow performs well away from regions of intense thermohaline circulation. The effect of having no mass transport through the Indonesian Passage is also investigated by evaluating the Sverdrup flow allowing for a net circulation around Australia. The fourth section explores the meridional overturning and vertical motion in the MS ocean states, with a view to detailing the modelled thermohaline circulation. The water mass distribution in the coupled model is described in the fifth section. Simulated basin-averaged temperature and salinity is compared with observed long-term mean distributions. Comparison is made with climatological ideas about the region of formation, strength, and fate of the World's major water masses. Finally, the last section covers the discussion and conclusions.

The coupled ocean–atmosphere and Sverdrup models

The coupled model

The coupled ocean–atmosphere model employed by MS has been well-documented in several recent publications (e.g., MS; Manabe et al., 1990, 1991). The model has a global coverage of the ocean and atmosphere, with a realistic approximation of ocean topography and continental boundaries. The oceanic component of the model is similar to the model described by Bryan and Lewis (1979), in which the simplified equations of motion are constructed by use of the Boussinesq, rigid lid and hydrostatic approximations (Bryan, 1969; Cox, 1984). The grid spacing (3.75 degrees longitude by 4.5 degrees latitude with 12 vertical levels) is such that the model resolves large-scale

oceanic circulations such as western boundary currents and subtropical gyres, but it cannot detail subgrid features such as mesoscale eddies. The atmospheric component of the model has annual mean insolation at the top of the model atmosphere, so no seasonal features can develop in air–sea interaction.

Since the thermal capacity of the entire atmosphere is roughly equal to the thermal capacity of the upper two metres of the global ocean, the atmosphere alone responds to climatic forcing at relatively short time scales. In contrast, the coupled ocean–atmosphere system takes a long time to reach an equilibrium state, with the ventilation of the deep ocean basins occurring over thousands of years. The method of asynchronous integration (Manabe and Bryan, 1969; Bryan, 1984) is employed to speed up the convergence of the coupled system to equilibrium.

MS found that two quasi-stable climate modes can exist depending on the initial state of integration of this coupled model. When the initial state has no deep water formation in the North Atlantic (i.e., a “collapsed” thermohaline circulation), none evolves during the integration, in spite of a surface fresh water flux adjustment that would tend to encourage NADW formation. In contrast, thermohaline overturning in the North Atlantic is maintained if it is present in the initial conditions. The essential features of the two climate modes have been detailed by MS and England (1991a). It is worth noting that whilst the two climate modes exhibit no systematic trend in temporal variability (MS), they become unstable after a somewhat lengthy integration (Stouffer, 1991, pers. commun.). It turns out that a topographic instability (Killworth, 1987) develops at very high latitudes in the Arctic Ocean (Stouffer, 1991, pers. commun.). Furthermore, Weaver and Sarachik (1991) show how a two-hemisphere ocean basin can ultimately yield a steady one-cell circulation in the meridional plane, even though the model ocean passes through an *apparently* stable period with a collapsed thermohaline circulation. For these reasons, we have chosen to refer to the MS climate modes as “quasi-stable” states.

Following the convention established in MS, we will refer to their quasi-stable states as Exper-

iments I and II; with Expt. I maintaining a strong thermohaline overturning in the North Atlantic and Expt. II having no deep water formation in the Northern Hemisphere. Experiment I is most like the present day real ocean, with deep water formation in the extreme Southern Ocean and the far North Atlantic. Experiment II is different to the “inverse conveyor belt” of Broecker et al. (1985), in that there is no deep water formation in either the North Atlantic or North Pacific. Experiment II is more like the “southern sinking mode” found in the idealised ocean model of Marotzke and Willebrand (1991), in that deep water is formed exclusively in the extreme Southern Ocean.

The Sverdrup model

Godfrey (1989) developed a Sverdrup model of depth-integrated flow that allows for circulation around islands. The linearised, time-independent, vertically-integrated momentum and continuity equations are used to derive the volume transport streamfunction Ψ of the Sverdrup circulation. The form of Ψ can be expressed as a function of the wind stress τ , namely

$$\Psi(x) = \int_{x_0}^x \frac{1}{\rho\beta} (\nabla_H \times \tau) dx' + \Psi(x_0). \quad (1)$$

where ρ is the water density, $\beta = df/dy$ is the latitudinal variation in the Coriolis parameter f , and ∇_H is the horizontal del operator. Conventionally, the Sverdrup mass transport streamfunction is calculated from eqn. (1) by integrating the curl of the wind stress westward along latitude lines from an eastern boundary. The boundary condition that there be no flow orthogonal to a rigid boundary requires Ψ to be constant (and by convention zero) along the eastern boundary (x_0).

In much of the World Ocean basins, a continuous eastern boundary makes the implementation of the Sverdrup model simple. For example, both the Atlantic and Pacific basins have continuous eastern boundaries from their northernmost latitudes to the Southern Ocean. However, the Indian Ocean is unbounded to the east at the latitudes of the Indonesian through-flow.

In the MS model, the only island that has a circulation around it is Antarctica, with just less than 100 Sv forming the Antarctic Circumpolar Current (ACC) in each experiment (England, 1991). There is no barotropic flow through the Indonesian Passage because there are not enough ocean grid points through the passage to solve the horizontal streamfunction. Instead, MS allow a baroclinic throughflow, in that heat and fresh-water are able to pass through the Indonesian Archipelago, it is only the depth-integrated flow of mass that must vanish. The Sverdrup model of Godfrey (1989) allows us to estimate the Indonesian throughflow that might exist if the barotropic streamfunction was also solved through the Passage in MS. If the pressure field is assumed to be continuous, the circulation around an island can be written in terms of the integral of wind stress around a closed path enclosing the island and the ocean bounded by the island and the nearest eastern boundary (de Szoeke, 1987; Godfrey, 1989). The island rule can then be written as

$$\Psi_I = \frac{1}{\rho(f_S - f_N)} \oint \tau \cdot ds, \quad (2)$$

where Ψ_I is the island value of the streamfunction, f_S and f_N are the values of the Coriolis parameter at the southern and northern limits of the island, and ds is the unit vector parallel to the path of integration.

The depth-integrated steric height (P_Z) relative to some depth of no motion (at $z = Z$) can also provide an estimate of the structure of horizontal mass transport. Godfrey (1989) developed a wind-driven estimate of P_Z by assuming Sverdrup interior flow and geostrophy of longshore flow along western boundary currents. The formulation used by Godfrey (1989) assumes no vertical motion through a depth of no motion surface $z = Z$ (usually set somewhere between 1300 m and 2500 m), so the deep thermohaline circulation is neglected in this estimation. This would threaten the Sverdrup estimate of P_Z in the North Atlantic of MS's Experiment I, where 12 Sv of NADW is transported downward to depths of about 1500 m. Because we have a complete description of all three velocity components in the MS model, there is not much gained

by computing the Sverdrup estimate of P_Z —its structure will be very much like the Sverdrup estimate of horizontal mass transport (England, 1991). In contrast, without a complete description of horizontal velocity, Godfrey (1989) needed to compare the Sverdrup estimates of P_Z with Levitus derived “observations” of P_Z , in order to

shed light on the Sverdrup estimates of depth-integrated flow.

Sverdrup model estimates of depth-integrated flow in MS

The wind stress fields alone determine the Sverdrup model estimate of depth-integrated

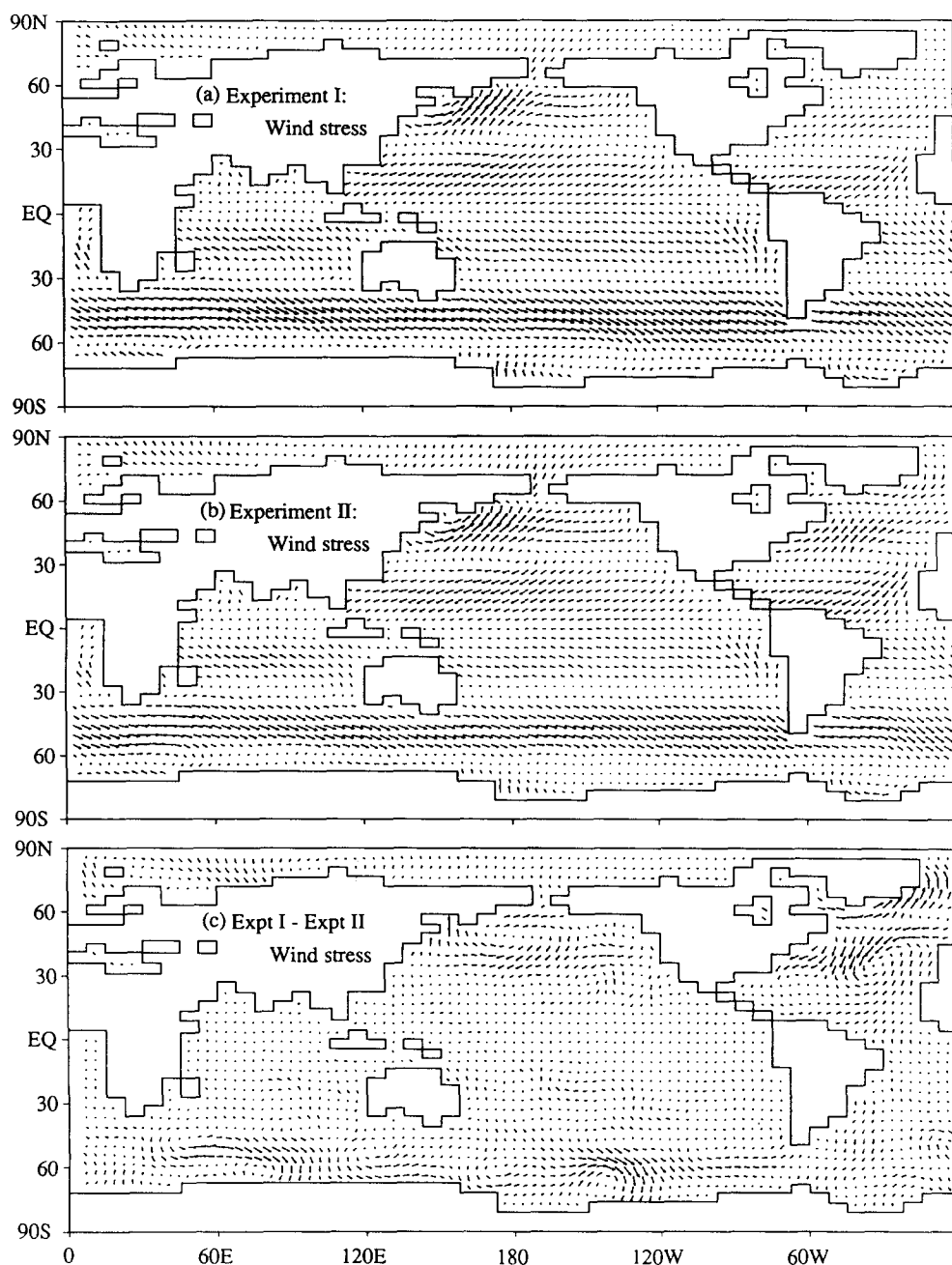


Fig. 1. Surface wind stress vectors in (a) Expt. I, (b) Expt. II and (c) the difference between Expts. I and II (i.e., I minus II). Vector scaling is such that the maximum vector length in (a) and (b) is 1.4 dynes/cm², whilst in (c) it is 0.5 dynes/cm².

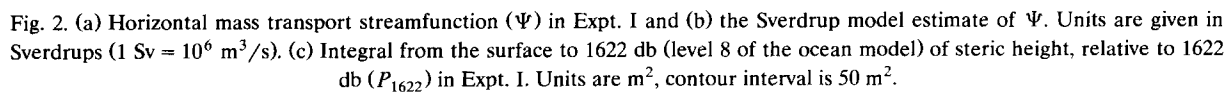
flow. So, it is certainly worth examining the MS wind stress fields in some detail. Figure 1 shows maps of wind stress vectors in each of Expts. I and II, as well as their difference. Each experiment captures the essential features of the global (annual mean) wind stress field. In the Southern Ocean, the winds blow slightly south of east at all longitudes. The tropics of each ocean basin have the Trade Winds blowing in the correct direction, and the convergence zones appear in the subtropics as in observation. The differenced map shows that the circumpolar westerlies are slightly stronger in Expt. I than in Expt. II, particularly in the south-west Indian and southern Pacific Oceans. Also, the map reveals that the North Atlantic has much stronger winds in the experiment without thermohaline overturning. This is linked to differences between the meridional temperature gradient and baroclinicity in the lower atmosphere of the two experiments. In fact, the wind stress field in the second experiment's North Atlantic resembles that of the North Pacific, which (in the Sverdrup model) would drive a similar ocean circulation. This suggests that the wind stress field reflects one of the essential distinctions between the two experiments; in Expt. II both Northern Hemisphere basins have strong meridional gradients of sea surface temperature driving a strong Ferrel cell in the atmosphere, whereas in Expt. I there is zonal asymmetry between the Atlantic and Pacific basins, with the thermohaline circulation moderating meridional temperature gradients (and hence wind stresses) in the North Atlantic.

A comparison between MS wind stress in Expt. I and the annual mean climatology of Hellerman and Rosenstein (1983, here after referred to as HR) reveals that the HR wind stresses are generally much stronger than those of MS. This could have to do with the fact that the MS model has annual mean insolation at the top of the model atmosphere, and as such, does not capture the strong winds characterising the winter hemisphere. In contrast, the HR annual mean is an average of monthly mean wind stresses observed over the global ocean. As an example, in the north-west Pacific Ocean, the HR annual mean winds are dominated by strong north-west winds

that blow off the Siberian desert in boreal winter. It should also be remembered that the HR wind stress climatology is now widely regarded to be too strong, primarily because the drag coefficient they use is systematically too high at low to moderate wind speeds (Chelton et al., 1990).

Nevertheless, the Sverdrup model can be readily applied to the coupled equilibria of MS, and comparison made with the exact values of Ψ that appear in the model ocean states. To be more explicit, applying the Sverdrup model involves taking the MS wind stress field and computing estimates of the volume transport streamfunction following eqn. (1). Notice that the most accurate Sverdrup model representation of the MS ocean has no Indonesian throughflow. Some comparison can be made with the findings of Godfrey (1989) and others, but the significant difference in wind strength between HR and MS should be kept in mind.

Before making a comparison between the actual MS horizontal mass transport and the Sverdrup model estimates, it is worth examining the processes that can contribute to a barotropic flow in the GFDL OGCM employed by MS. By examining the equations for the external mode of velocity, it is apparent that there are only three ways to drive a barotropic flow in the MS ocean. Firstly, a nonlinear interaction between baroclinic modes of velocity can contribute to the barotropic mode. This term is negligible in coarse resolution models such as the one employed by MS. Secondly, surface and bottom stresses can set up a barotropic flow. And thirdly, the so-called joint effect of baroclinicity and relief (JEBAR) can drive a barotropic circulation. JEBAR only contributes to the external mode of velocity in regions where there is a gradient in topography orthogonal to a gradient in density (Hsieh and Gill, 1984). So, in a deep flat-bottomed coarse resolution ocean GCM with only thermohaline forcing, the barotropic flow will be virtually zero everywhere at all time. In the MS model, it will primarily be the surface wind stress and JEBAR that drives the horizontal mass transport. On shallow continental shelves, particularly near western boundary currents, the bottom stress may also contribute significantly to the external mode.



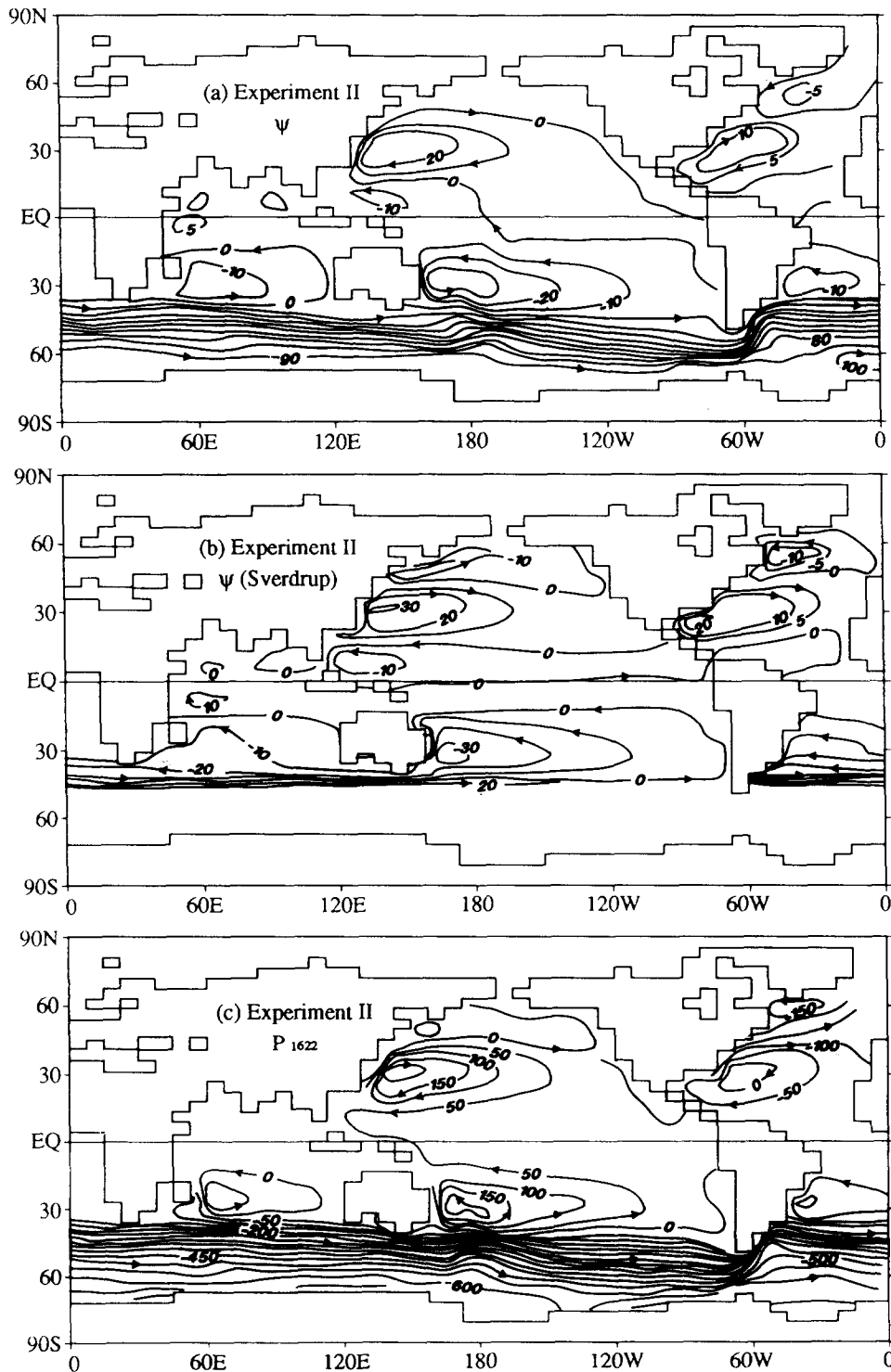


Fig. 3. (a) Horizontal mass transport streamfunction (Ψ) in Expt. II and (b) the Sverdrup model estimate of Ψ . Units are given in Sverdrups ($1 \text{ Sv} = 10^6 \text{ m}^3/\text{s}$). (c) Integral from the surface to 1622 db (level 8 of the ocean model) of steric height, relative to 1622 db (P_{1622}) in Expt. II. Units are m^2 , contour interval is 50 m^2 .

The Sverdrup model only includes the effects of the surface wind stress on the barotropic flow.

Sverdrup estimates of Ψ in the two MS experiments are shown in Figs. 2 and 3. Included in these figures for comparison are maps of actual horizontal mass transport streamfunction and depth-integrated steric height relative to 1622 db (level 8 of the model ocean) in each MS experiment. The reader is referred to Table 1 and Godfrey (1989) for the HR derived Sverdrup estimates of Ψ in the real World Ocean. A comparison between the MS Sverdrup flow and that derived by Godfrey (1989) essentially amounts to a comparison between MS wind stresses and the HR climatology (England, 1991), because the Sverdrup model employed in this study is exactly that of Godfrey (1989). Godfrey (1989) also presents figures showing depth-integrated steric height distributions calculated from the Levitus (1982) annual mean climatology. His map of depth-integrated steric height relative to 1500 db is very similar to the distribution shown for Expt. I (Fig. 2c), and so is not presented here.

The actual horizontal streamfunction Ψ in MS is calculated by integrating the depth-integrated u -component of mass transport from the northernmost grid points down to the required cell. That is,

$$\partial_y \Psi, \partial_x \Psi = \rho \int_{-H}^0 (-u, v) dz, \quad (3)$$

TABLE 1

Transports in Sv ($= 10^6 \text{ m}^3/\text{s}$) of the major western boundary currents and the Drake Passage and Indonesian throughflows computed for the Manabe and Stouffer states from the exact horizontal velocity fields ($I_{(u,v)}$, $II_{(u,v)}$), the wind stress driven Sverdrup model (I_τ , II_τ), and the Sverdrup model with Indonesian Passage open ($I_{\tau(\text{IP open})}$, $II_{\tau(\text{IP open})}$). Also shown is the Sverdrup transport estimates using the Hellerman and Rosenstein annual mean climatological wind stress (HR) with Indonesian Passage open

Current	$I_{(u,v)}$	I_τ	$I_{\tau(\text{IP open})}$	$II_{(u,v)}$	II_τ	$II_{\tau(\text{IP open})}$	HR
Gulf Stream	22	17		17	21		29
Labrador	20	7		8	15		46
Kuroshio	27	27		30	31		55
Oyashio	2	17		5	25		39
Brazil	15	19		16	18		30
Mindanao	11	14		12	15		23
East Australia	39	33	17	40	34	17	20
Somali	8	13	6	8	13	6	26
Agulhas	17	14	31	20	15	32	46
Indo. thr'flow	0	0	16	0	0	17	18
Drake Passage	90	30		96	40		114

where Ψ is the horizontal streamfunction, ρ the water density, u the east-west velocity, v the north-south velocity, H the depth of the ocean and x, y, z the east-west, north-south and vertical components, respectively. The depth-integrated steric height relative to some assumed depth of no motion $z = Z$ is calculated as

$$P_Z = \frac{1}{\rho_0 g^2} \int_{p(Z)}^0 \int_{p(Z)}^{p(z)} \delta(S, T, p') dp' dp, \quad (4)$$

where ρ_0 is a reference density, g is gravity and $\delta(S, T, p)$ is the specific volume anomaly for water of temperature T and salinity S , at pressure p . The value of $\delta(S, T, p)$ is computed using standard algorithms. Values of P_Z were computed for several depths of no motion from $Z = 1131 \text{ m}$ (level 7 of the model) through to $Z = 3721 \text{ m}$ (level 11 of the model). Only the values of P_{1622} are presented here for comparison, because in the region of the Sverdrup model (i.e., north of the latitude of Cape Horn), it is a reasonable depth of no motion except in the North Atlantic of Expt. I. This has to do with the location of deep water formation in the MS models; it occurs in the extreme Southern Ocean of each experiment, and the North Atlantic of Expt. I.

In both Expts. I and II, the Sverdrup model gives a good representation of the mass transport streamfunction in most areas of the MS World

Ocean. Table 1 gives a summary of the mass transport values of the major currents in the MS and Sverdrup models respectively. Both the East Australian Current (EAC) and the Kuroshio Current are well-represented by the Sverdrup model, as is the 10 Sv circulation just north of the equator in the Pacific Ocean (the Mindanao Current). However, the wind stress model predicts a strong Oyashio Current in each experiment (17 Sv, 25 Sv respectively), whilst the actual MS model values of Ψ remain small (2 Sv, 5 Sv). Godfrey (1989) also notes that his Sverdrup model estimate of the Oyashio is somewhat too strong (see Table 1). In the MS model, it must be that JEBAR and/or bottom stresses are generating a transport in the opposite sense to the wind-driven flow. Examination of density sections at depth indicate significant deep density gradients in the far North Pacific. Coupled with the topographic gradients that exist in the MS bathymetry, this would generate a barotropic flow through JEBAR.

The ACC in the MS experiments flows mostly south of the latitude of cape Horn, and as such, is not prominent in the Sverdrup model of mass transport. However, if one assumes that the ACC flows northward as the Malvinas Current after passing through the Drake Passage, this provides a Sverdrup estimate of the strength of the Circumpolar Current. This gave Godfrey (1989) the opportunity to estimate the strength of the ACC as 128 Sv. Were this assumption to be made in the present study, the Sverdrup model would estimate the ACC as 30 Sv and 40 Sv in the two experiments. This at first appears much less than the actual MS model ACC strengths of 90 Sv and 96 Sv. However, careful examination of Figs. 2a and 3a shows that only about 50–60 Sv of the ACC flows north of the latitude of Cape Horn, not much more than the Sverdrup model estimates.

Depth-integrated flow patterns in the Indian Ocean are remarkably well-represented by the Sverdrup model except in the region south of the Agulhas Current, where the model predicts that the Agulhas Current joins a westward jet originating in the south-west Pacific off Australia. The actual MS values of Ψ show the Agulhas Current flowing as part of a subtropical gyre, and no

westward flow at all in the south Indian Ocean. Godfrey (1989), Welander (1959) and Evenson and Veronis (1975) all find this erroneous westward jet in their studies of Sverdrup circulation.

In the Atlantic basin, the Brazil Current is accurately represented by the Sverdrup model, although the intense westward jet from the Agulhas retroflection swamps the region, and turns southward at the east coast of South America, to join the ACC. In the North Atlantic, the Sverdrup model appears to capture the *structure* of flow rather accurately in both experiments, even though the North Atlantic of Expt. I is strongly driven by a deep thermohaline circulation. However, it is apparent that the wind-driven model underestimates the Gulf Stream and North Atlantic polar gyre of Expt. I. This shortfall cannot be connected with bottom stresses in the MS ocean, for these would tend to slow down the barotropic flow in western boundary currents. So, it can only be connected with the thermohaline circulation (through JEBAR), since the nonlinear interaction of baroclinic velocity modes is negligible at coarse resolution. It turns out that there are significant topographic and deep density gradients in the North Atlantic of Expt. I, confirming that JEBAR must be prevalent in the simulated barotropic flow.

The map of depth-integrated steric height in Expt. I (Fig. 2c) shows a very broad geostrophic current flowing from the Gulf Stream across to the Norwegian Sea. This corresponds with the surface manifestation of the thermohaline circulation in the run with NADW formation. This is reminiscent of the surface drift vectors presented by MS (see their fig. 13). It is also very similar to the observed patterns of P_z calculated by Godfrey (see his fig. 6). Clearly, a Sverdrup model of depth-integrated flow is inappropriate in the North Atlantic of Expt. I, since the large-scale circulation is driven by gradients in density rather than simple wind forcing. In the second experiment on the other hand, the North Atlantic behaves much like the North Pacific, with two major gyre circulations and no deep water formation.

It is interesting to examine the distribution of P_z in the North Atlantic of Expt. I when the depth of $z = Z$ is much closer to a depth of no

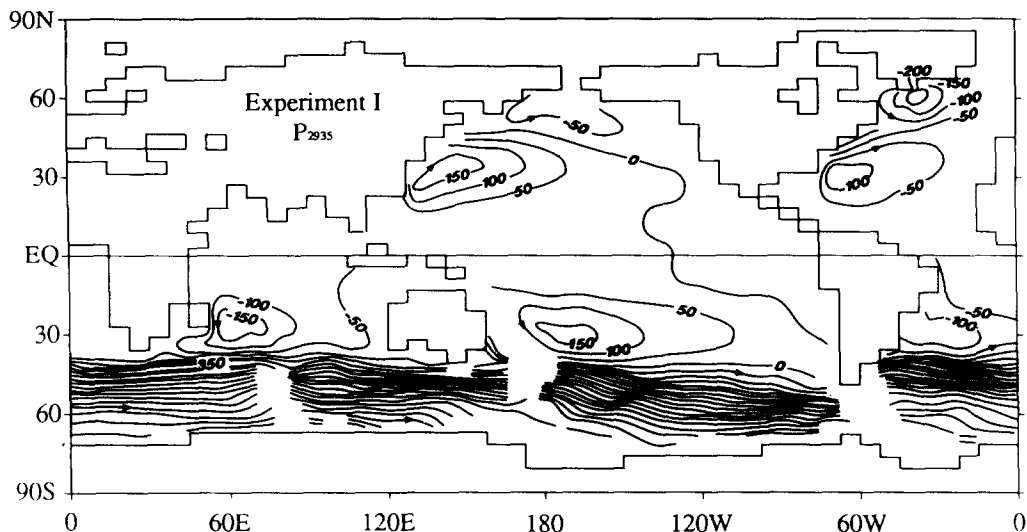


Fig. 4. Integral from the surface to 2935 db (level 10 of the ocean model) of steric height, relative to 2935 db in Expt. I. P_{2935} is undefined in regions where the model bathymetry is less than 10 grid levels deep. Units are m^2 , contour interval is 50 m^2 .

motion. MS showed that the penetration of NADW existed to depths of about 2500 m (see their fig. 12). Figure 4 shows the depth-integrated steric height relative to 2935 db (level 10 of the MS model) in Expt. I. It is clearly more similar to the actual depth-integrated flow represented in Fig. 2a. This is because P_z reflects the depth-integrated geostrophic flow relative to a depth of no motion at $z = Z$. In Expt. I, a broad geostrophic flow in the surface layer feeds warm

saline tropical water into the Norwegian Sea (Fig. 2c). However, a return geostrophic flow of NADW appears at greater depths (1000 m–2500 m), which is reflected in the barotropic flow shown in Fig. 2a. So, by going to a true depth of no motion, the distribution of P_z more closely reflects the actual depth-integrated flow.

One simplification of the MS model is to have no barotropic mass transport through the Indonesian Passage. The effect of this can be investi-

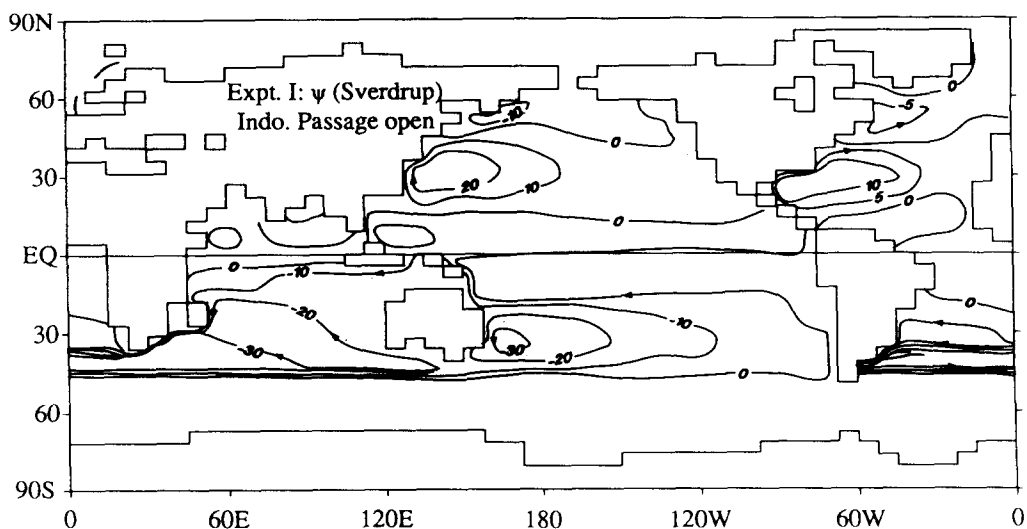


Fig. 5. Sverdrup model estimate of horizontal mass transport streamfunction (Sv) in Expt. I allowing for an Indonesian throughflow.

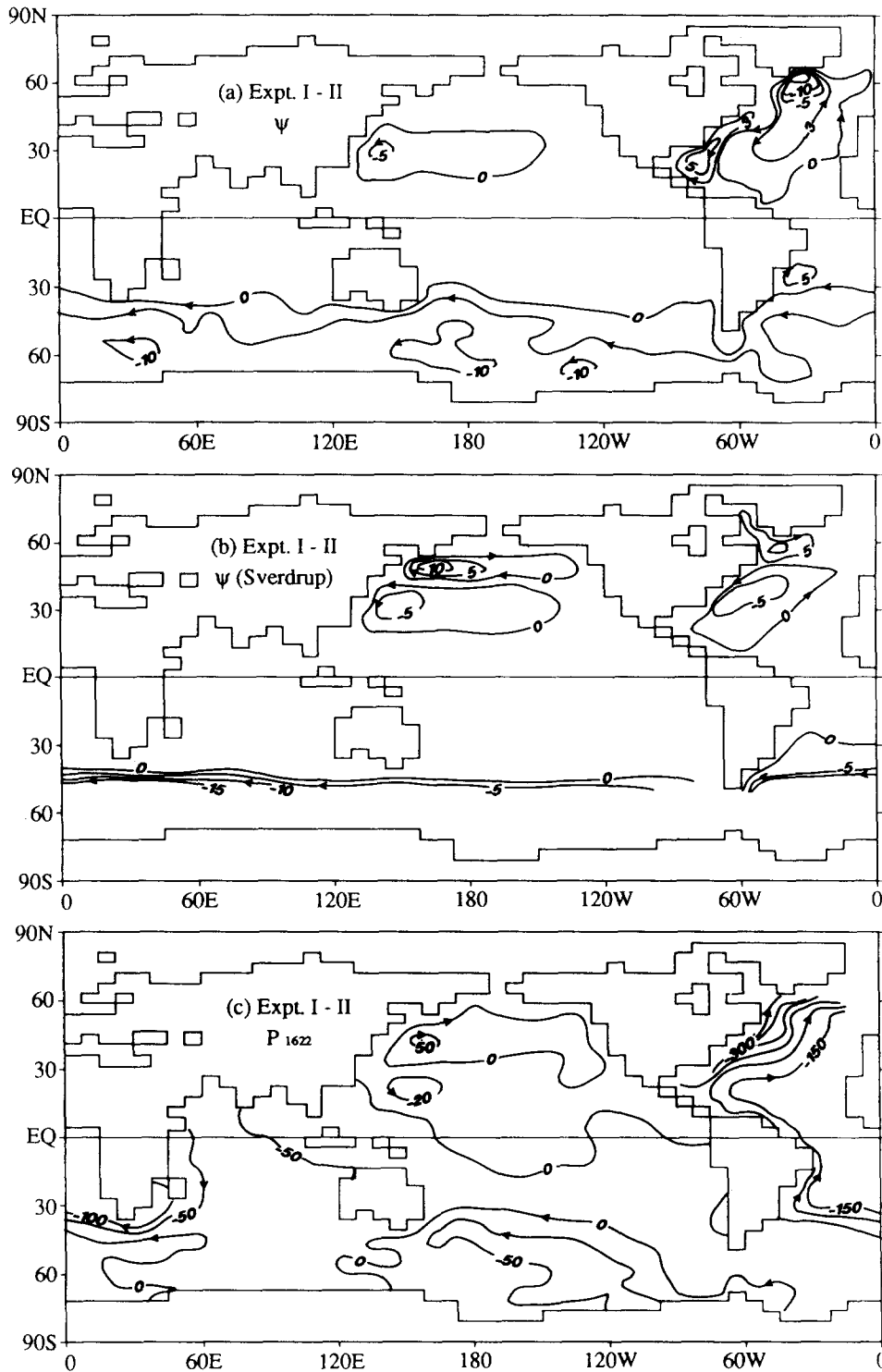


Fig. 6. (a) Difference (Expt. I minus Expt. II) in horizontal mass transport streamfunction and (b), that estimated by the Sverdrup model. Units are given in Sverdrups. (c) The difference in P_{1622} between the two experiments. Units are m^2 .

gated by computing the Sverdrup model allowing for an Indonesian throughflow. Figure 5 shows wind-driven estimates of Ψ were the Indonesian Passage open to mass transport in Expt. I (see also Table 1). The most dramatic change from the earlier Sverdrup estimates appears in the Indonesian Passage, where 16 Sv now flows from the Pacific basin into the Indian Ocean, which is very close to recent estimates of the Indonesian throughflow (e.g., 10–13 Sv, Godfrey, 1989; 16 Sv, Chelton et al., 1990; 17 Sv, de Szoeke, 1987). Furthermore, the 16 Sv throughflow weakens the EAC from 33 Sv to 17 Sv. Once the throughflow enters the Indian Ocean it feeds the equatorial current, and strengthens the Agulhas Current from 14 Sv to 31 Sv, which is more realistic [Gill and Schumann (1979) estimate that the Agulhas Current transports 60–70 Sv]. Also, notice that the weak Somali current (13 Sv) estimated by the original Sverdrup model is swamped by the new equatorial current. The wind-driven model estimates remain unchanged in the Atlantic and North Pacific basins, by nature of the integration paths used.

Because the Sverdrup model is completely linear, the differenced depth-integrated flow can be investigated by evaluating the Sverdrup model on the differenced wind stress field. Figure 6 shows the difference in Ψ between the two experiments and the Sverdrup estimate based on the wind stress difference. A similar figure is also presented for the difference in depth-integrated steric height. It seems that the essential differences in the depth-integrated flow field are related to differences in wind stress in the North Pacific and Southern Oceans (north of the Drake Passage gap). For example, the difference in ACC strength (or more accurately, Malvinas current strength) is predicted by the Sverdrup model, as are the stronger North Pacific gyre circulations in the second experiment. In contrast, the Sverdrup model does little in terms of explaining the difference in flow fields in the North Atlantic. In fact, the Sverdrup model predicts that the strength of the Gulf Stream and subpolar gyres should be stronger in the second experiment, when they are actually weaker. This is because the circulation in the North Atlantic of Expt. I is driven signifi-

cantly by the ocean's thermohaline field (through JEBAR), rather than by surface wind stress forcing alone (as the Sverdrup model would have it). So, it would seem that the Gulf Stream in Expt. I behaves quite differently to the other poleward flowing western boundary currents in the MS study—although it is predominantly wind-driven, it includes a significant component of JEBAR forced transport.

Finally, it is worth noting that the difference in P_{1622} (Fig. 6c) gives a good representation of the depth-integrated flow field for the source water of NADW formation. Water is drawn from the Indian Ocean via the Agulhas Current around the Cape of Good Hope, where it travels westward to the east coast of South America. From there, the integrated pressure field shows that water is transported northward along the east coast of the Americas and into the Gulf Stream, where it forms a broad current that takes low latitude water into the Norwegian Sea. Because the steric height is only integrated down to $z = 1622$ m, this figure does not reveal the flow path once the deep water has been formed. That would be revealed in a picture of depth-integrated flow from the ocean floor to a grid level depth of say 1130 m.

Meridional overturning and vertical motion in MS

An entirely different perspective on the oceanic circulation is given by the zonally-integrated mass transport in the meridional plane. This net transport Ψ is well-defined as a global statistic and in regions bounded by meridional barriers. It is computed as

$$\partial_z \Psi, \partial_y \Psi = a \rho \int_0^\lambda (-v, w) \cos \phi \, d\lambda, \quad (5)$$

where Ψ is the meridional mass transport streamfunction, v the north–south velocity, w the vertical velocity, a the radius of the earth, ρ the water density, ϕ latitude and λ longitude in degrees. Following eqn. (5), the meridional circulation in the ocean was computed at each depth level, and zonally-integrated to give a measure of global meridional mass transport. The resulting

patterns of global meridional circulation in Expts. I and II (and their difference), is shown in Fig. 7. The total overturning can be further diagnosed by computing the transport component in each zonally bounded ocean basin (that is, away from regions where the ocean is free to exchange mass zonally). Figure 8 shows the meridional overturning in each ocean basin of Expt. I and Fig. 9 shows the differenced circulation between the two experiments.

Near the sea surface of each hemisphere in each run, the meridional circulation is dominated

by Ekman transport in the planetary boundary layer. At low latitudes in the Trade Wind zone, the Ekman transport is poleward, with a global net mass flux of 29 Sv and 28 Sv southward, and 22 Sv and 25 Sv northward in Expts. I and II respectively. Comparing the two climate modes of MS, this near-surface poleward transport is stronger in the North Atlantic and South Indian Oceans in Expt. I (Fig. 9a,b). However, in Expt. II a stronger Ferrel cell in the atmosphere drives a stronger tropical overturning in the North Pacific Ocean (Fig. 9c). The massive near-surface

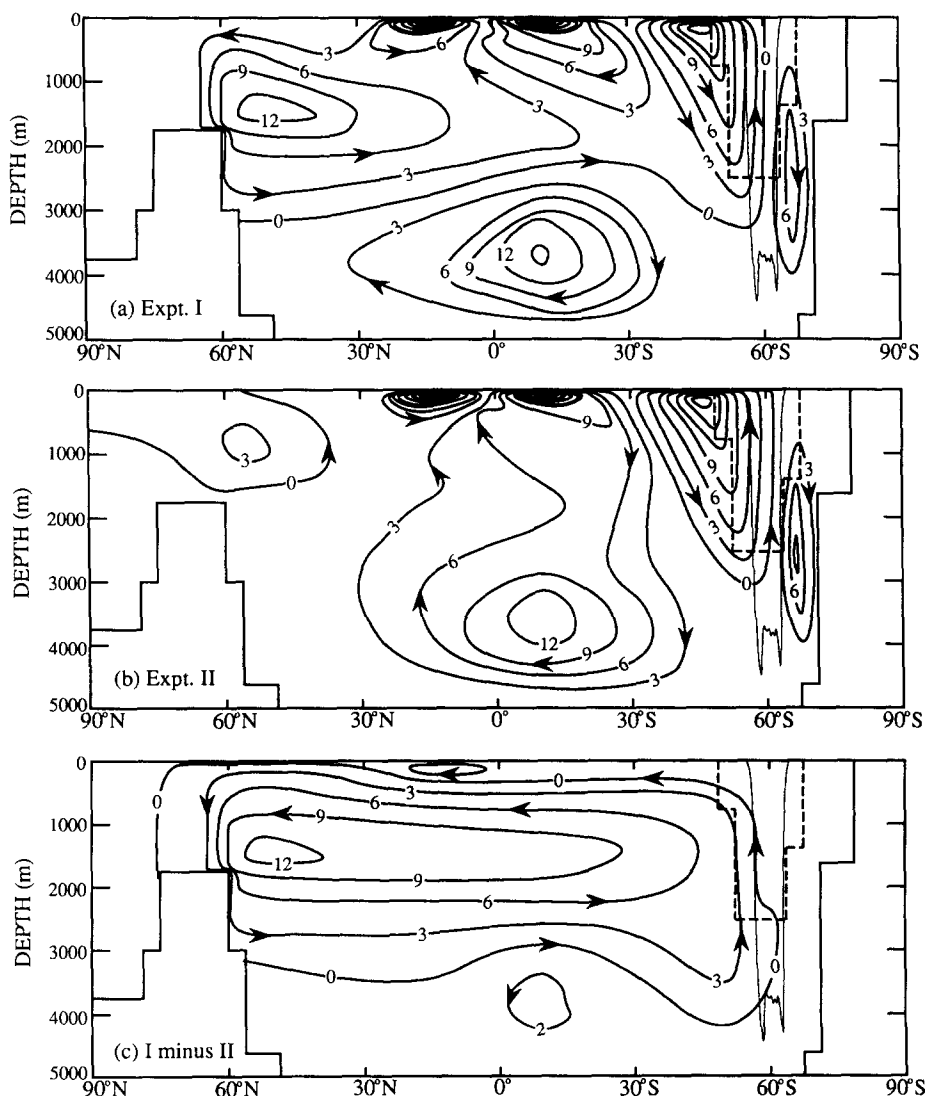


Fig. 7. Global meridional overturning streamfunction in (a) Expt. I, (b) Expt. II and (c) the difference between Expts. I and II (i.e., I minus II). Transports are shown in Sverdrups. The dashed line near 60°S denotes the model's representation of the Drake Passage, whereas the fine contour shows the actual Drake Passage bathymetry.

transport away from the equator is compensated by a return flow in the tropical thermocline, and concentrated upwelling at the equator. The con-

vergence of water at 30°S leads to the formation of Central Water in the model ocean. Of course, Figs. 7 and 8 do not reveal the exact location of

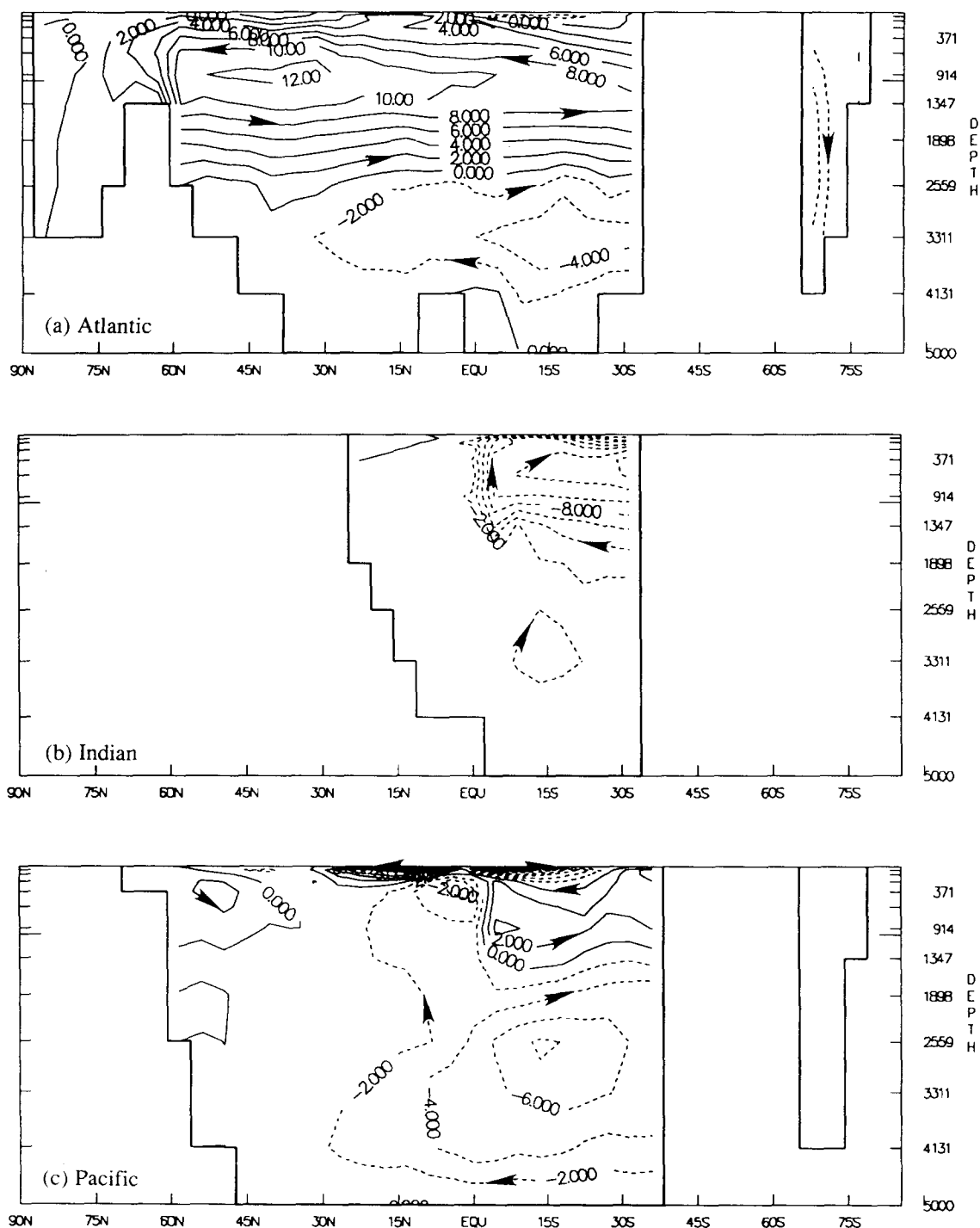


Fig. 8. Zonally-averaged meridional overturning in the (a) Atlantic, (b) Indian and (c) Pacific basins of Expt. 1. Contour interval is 2 Sv. No streamfunction can be defined in regions where the ocean is free to exchange mass zonally.

Central Water formation and thermocline ventilation in the MS oceans, because they only show zonally-averaged meridional circulation.

In the Northern Hemisphere of Expt. I, some of the low-latitude Ekman transport extends further north than 30°N, joining up with the deep

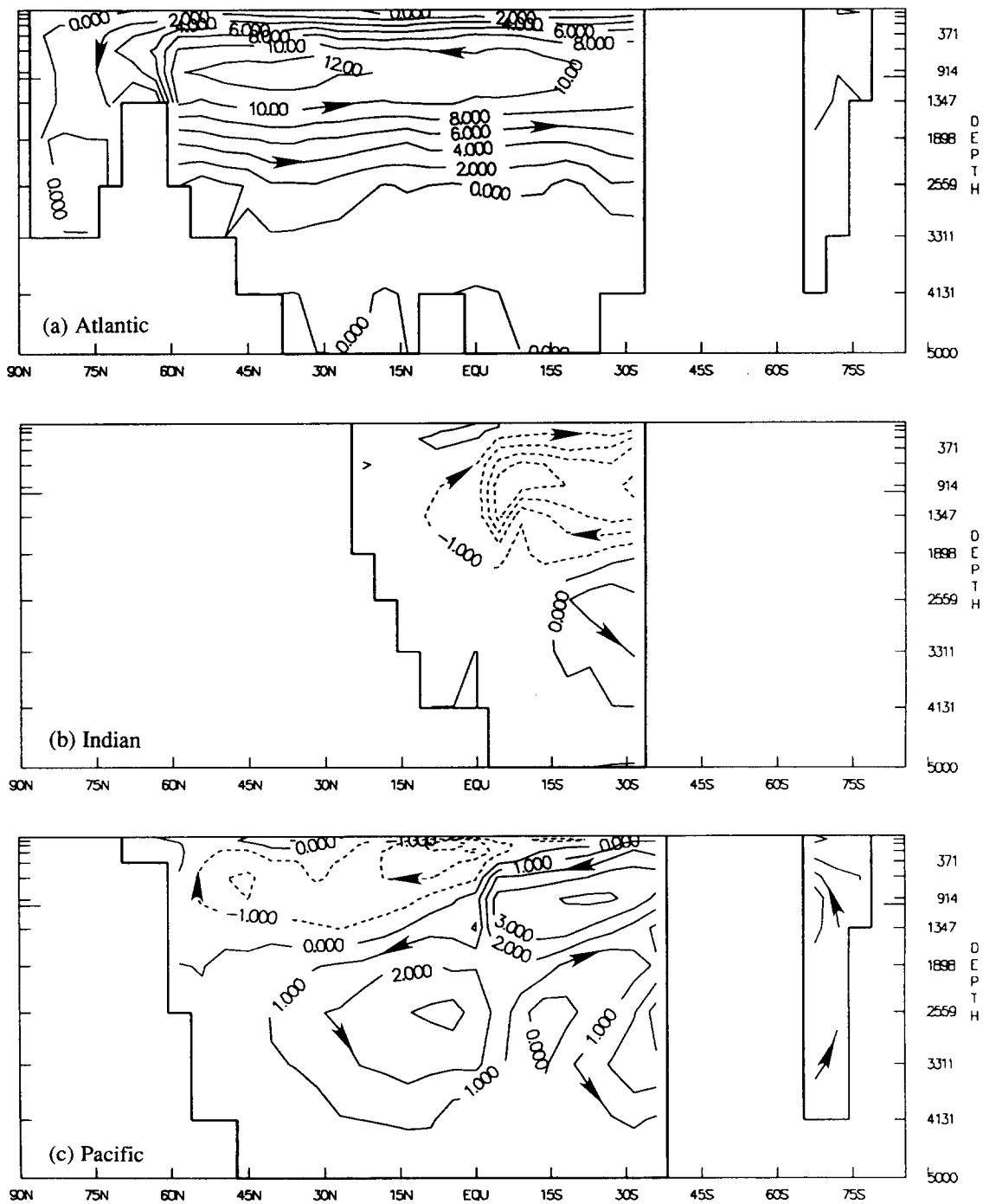


Fig. 9. Difference (Expt. I minus Expt. II) between the zonally-averaged meridional overturning in the (a) Atlantic, (b) Indian and (c) Pacific basins. Contour interval is 2 Sv in the Atlantic section and 1 Sv in the Pacific and Indian sections. No streamfunction can be defined in regions where the ocean is free to exchange mass zonally.

overturning cell centred at 45°N. This deep ocean circulation occurs only in the North Atlantic Ocean of Expt. I (Figs. 7, 8), with strong near-surface northward transport up to 60°N (where NADW formation and sinking occurs), and a southward return flow below a depth of 1 km. From the Atlantic basin section of Ψ (Fig. 8a), it appears that only 8 Sv of the NADW formed flows into the Southern Ocean, the rest being upwelled in the tropical Atlantic. In the second experiment, all of the North Atlantic low latitude Ekman transport returns in the tropical thermocline after sinking at about 30°N (Fig. 7b) and no significant thermohaline circulation is apparent. Notice, however, that in each experiment (Figs. 8a, 9a) a deep overturning cell centred just south of the equator transports more than 4 Sv of bottom water from the Southern Ocean into the deep North Atlantic. This means that even in Expt. I, the ventilation of the deep North Atlantic is not originating from the thermohaline overturning of NADW.

At the latitudes of the westerlies (40–60°S, and to a lesser extent, 40–50°N, from Fig. 1), the Ekman transport in the planetary boundary layer is equatorward. In the Northern Hemisphere, where the oceans are always bound to the east and the west, the Ekman transport under the westerlies can be compensated by a shallow geostrophic return flow in the upper thermocline. In contrast in the Southern Hemisphere, where the model ocean is zonally unbounded between latitudes of 51°S and 64°S (i.e., at the latitudes of the Drake Passage), the strong equatorward transport under the westerlies is compensated by a deep cell (recently termed the “Deacon Cell”) extending well below the thermocline (Figs. 7a,b). Near-surface water at 40°S (north of the ACC) is downwelled to 1000–2500 m depth, flows southward geostrophically across the sill of the Drake Passage and is upwelled south of the ACC. Deacon (1937) originally suggested the existence of deep downwelling equatorward of the Circumpolar Current and deep upwelling poleward of the current on the basis of water mass analysis of the hydrography measured during the *Challenger* expedition.

One important aspect of the Deacon Cell is that its strength and shape is strongly determined by the model's bathymetry in the Drake Passage, because there can be no significant geostrophic return flow in the absence of continental boundaries (see Fig. 7a,b). In reality, the Drake Passage is somewhat narrower than the barrier-free zone in the MS model (Fig. 7). Indeed, many coarse resolution World Ocean models have artificially widened the Drake Passage in order to adequately resolve features of the ACC (e.g., Toggweiler et al., 1989a,b; Manabe et al., 1990). The problem with this approach is that it prohibits the strong Ekman transport under the westerlies from being compensated by a shallow return flow, because the Drake Passage has been artificially extended northward into the latitudes of strong zonal winds. So, the problem is not the width of the Drake Passage per se, but its unrealistic northward extent (in this case 51°S, compared to 56°S in the real ocean). A World Ocean model has been recently integrated with the Drake Passage not so infringing on the latitudes of strong near-surface wind-driven flow (England, 1992). The Deacon Cell remains as deep as it was in the control run, but it becomes less intense with depth, because more of the near-surface flow is compensated at shallow (bounded) levels. This serves to improve the quality of the World Ocean model in reproducing observed temperature and salinity fields in the Southern Ocean (England, 1992).

In addition to the deep wind-driven cell described above, there is another cell circulating in the immediate vicinity of Antarctica (in the opposite direction) where deep convective overturning prevails. This corresponds with the vertical motion associated with the formation of the model's bottom water. In both experiments, the formation of bottom water occurs via the thermohaline circulation (reflected in the maps of meridional overturning) and the deep convective adjustment processes included in the MS model. Figure 8 shows that in Expt. I much of the vertical motion occurs in the Weddell Sea, with only a minor contribution from the extreme South Pacific. A slightly stronger rate of bottom water formation

in Expt. II (Fig. 7) is due to more intense vertical motions in the Ross Sea in that run (Fig. 9c). Even though the *globally* averaged overturning shows no continuous flow from the cell forming bottom water into the deep tropical overturning circulation (Fig. 7a,b), sections of horizontal velocity indicate a continuous northward transport of bottom water in the far South Atlantic originating from the Weddell Sea. Whilst the bottom water overturns in the immediate vicinity of Antarctica, it will be seen in the next section that the air–sea interaction can be traced to the sur-

face at 60°S. This leaves the MS bottom water too fresh and warm.

Whilst a map of meridional overturning reveals the zonally-integrated circulation in the latitude–depth plane, it does not detail how the vertical motion is distributed with longitude. To find out how the net circulation is distributed we need to go to horizontal sections of vertical velocity. Figure 10 shows the distribution of vertical velocity at depths of 51 m and 595 m in Expt. I.

The vertical velocity just below the first layer (Fig. 10a) is simply the velocity required to com-

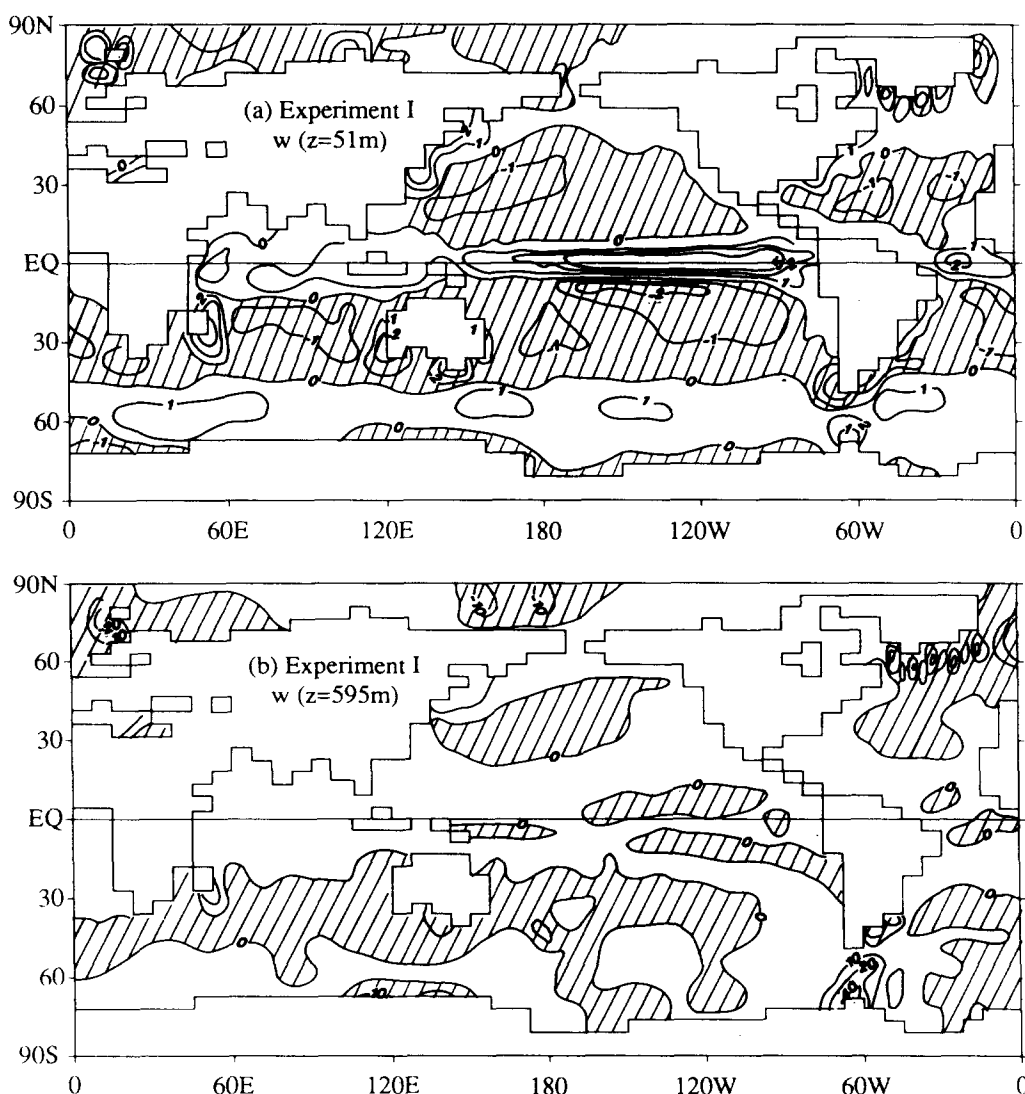


Fig. 10. Vertical velocity at a depth of (a) 51 m and (b) 595 m in Expt. I. Downward motion is denoted by stippled areas. Contours are drawn at 0, 1, 2, 5 and $10 \times 10^{-6} \text{ m/s}$ in (a) and at 0, 10, 20 and $40 \times 10^{-6} \text{ m/s}$ in (b).

pensate the divergence in the first layer, primarily made up of wind-driven Ekman divergence. For this reason, strong upwelling occurs along the equatorial waveguide of each ocean basin, and most significantly in the eastern Pacific. Downward motion near the surface prevails over the subtropics and mid-latitudes, except in the cells adjacent to side boundaries; and in particular, western boundaries, where intense upwelling is required to compensate strong poleward currents. There is near uniform upwelling across the Southern Ocean in the surface layer, except at some of the cells adjacent to Antarctica and in the Weddell Sea.

At deeper levels of the model ocean, the vertical motion is not only controlled by wind-driven Ekman divergence in the upper layers, but also by the thermohaline circulation, and in particular, the sinking of dense water in regions of water-mass formation. Figure 10b shows the vertical velocity distribution at a depth of 595 m. The most intense vertical motions are found at the cells adjacent to side boundaries, in the Drake Passage, and (in the case of Expt. I) in the North Atlantic. The distribution of vertical velocity is highly variable around regions of strong upwelling and downwelling, particularly at high latitudes. For example, in the North Atlantic of Expt. I, there is an *average* downward velocity of 2.2×10^{-6} m/s along 60°N, linked with the sinking of NADW. However, along 60°N the velocities alternate between being strongly positive (order 10^{-5} m/s upwelling) and strongly negative (order 1.5×10^{-5} m/s downwelling) from one grid point to the next. This has to do with the Fourier filtering employed by ocean GCM's at high latitudes (to combat the effect of converging meridians), which tends to produce artificial two-grid point oscillations in the vertical velocity field.

In the subtropical convergence zone in the Southern Hemisphere (30°–45°S) there is downwelling on a zonal average in each experiment (Figs. 7a,b). In the first experiment, the water that sinks at 30°–35°S tends to recirculate towards the tropical thermocline, to be upwelled at the equator. This sinking corresponds with the formation of Central Water and the ventilation of

the ocean's thermocline (Luyten et al., 1983). In the second experiment, however, the formation of Central Water is less clear. The sinking of surface water at 30°–35°S joins up with the deep overturning cell centred just south of the equator at 3500 m depth. This deep ventilation of subtropical water is quite unrealistic and is probably linked to the absence of deep water formation in the North Atlantic of Expt. II.

In the first experiment, the subduction in the subtropical convergence occurs in the south Indian and western South Pacific Oceans, as well as adjacent to the western boundary of South America in the confluence region of the Malvinas and Brazil Currents (Fig. 10b). Furthermore, there is a "shadow zone" (i.e., a region not reached by ventilated fluid) in the eastern South Pacific (denoted by the region of weak upward motion). This corresponds extremely well with the observed regions of Central Water formation and thermocline ventilation in the Southern Hemisphere (Sprintall and Tomczak, 1992).

The location of subduction at 30°–45°S show some distinct differences in the two experiments. In the first experiment, there is a significant source of Central Water in the South Indian Ocean, with water being downwelled in a broad band stretching from the South Atlantic past South Africa across to Australia. In contrast, the second experiment (not shown) has sinking in only some areas of the South Indian Ocean and significant downwelling off the coast of Southern Chile. So the eastern South Pacific is well ventilated in Expt. II, whilst in Expt. I it behaves as an unventilated shadow zone.

The water that sinks at 35°–45°S feeds the deep wind-driven cell described earlier; it downwells north of the Drake Passage, moves southward at the base of the Passage, and upwells just south of the ACC. The area of most intense upwelling in each run is in the Drake Passage itself (Fig. 10) because it is here that the deep ACC is forced upwards by the topography of the ocean floor. The upward movement continues from the base of the Drake Passage toward the surface, with vertical velocities reaching up to about 4×10^{-5} m/s at a depth of 595 m. The upwelling occurs at all latitudes of the Passage;

from Cape Horn intensifying to maximum upwelling off the Antarctic Peninsula. Both runs also upwell just eastward of the Drake Passage

(north of the Weddell Sea). The maps of differenced w at 595 m (not shown) reveal that the run with NADW formation upwells significantly more

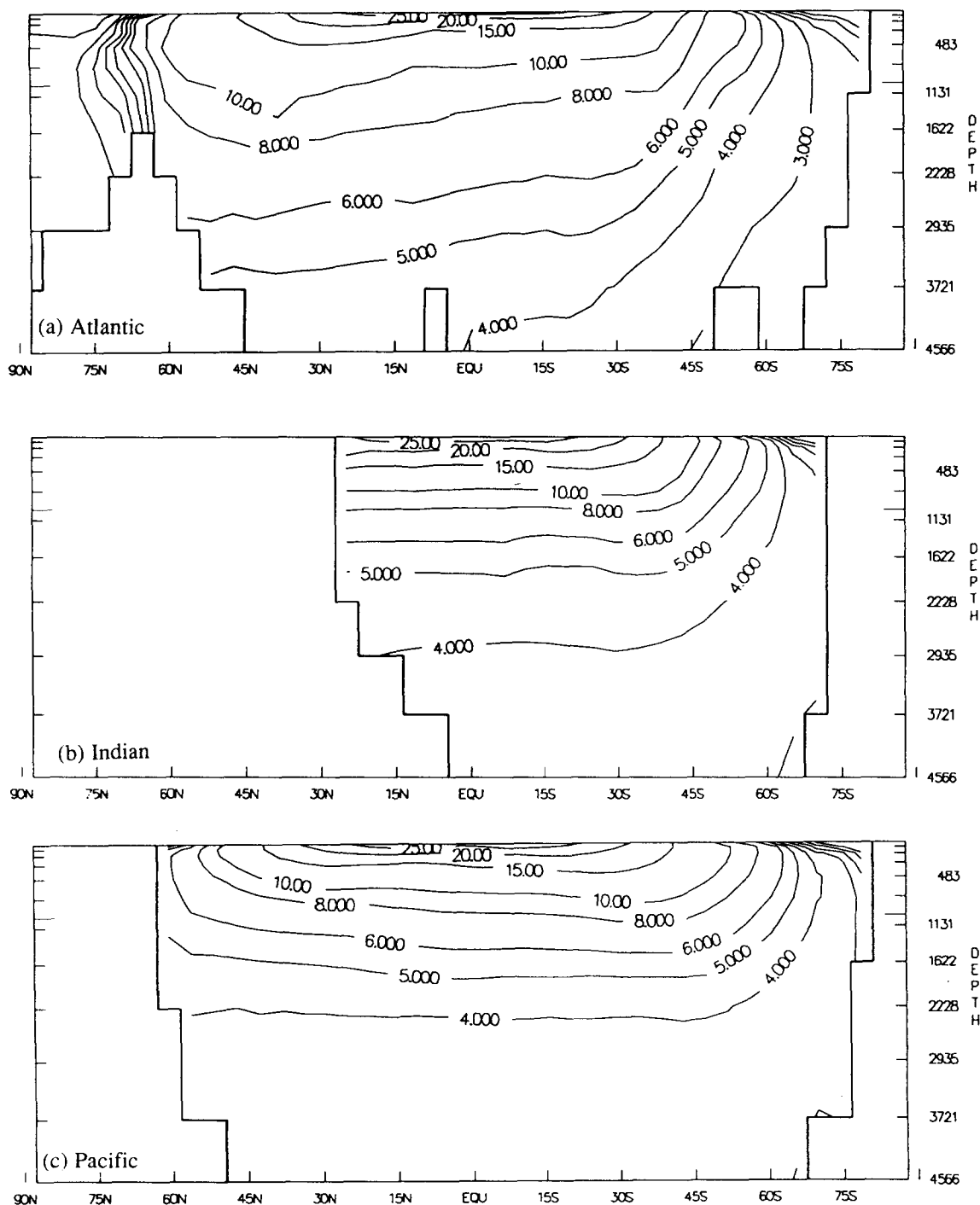


Fig. 11. Zonally-averaged potential temperature ($^{\circ}\text{C}$) in the (a) Atlantic, (b) Indian and (c) Pacific basins of Expt. I. Contours are drawn at 1°C intervals in the deep ocean.

water in the South Indian Ocean south of the Cape of Good Hope, but significantly less in the far South Atlantic.

The vertical velocity sections at $z = 2559$ m (not shown) reveal that the deep overturning of the model's bottom water occurs in the Weddell

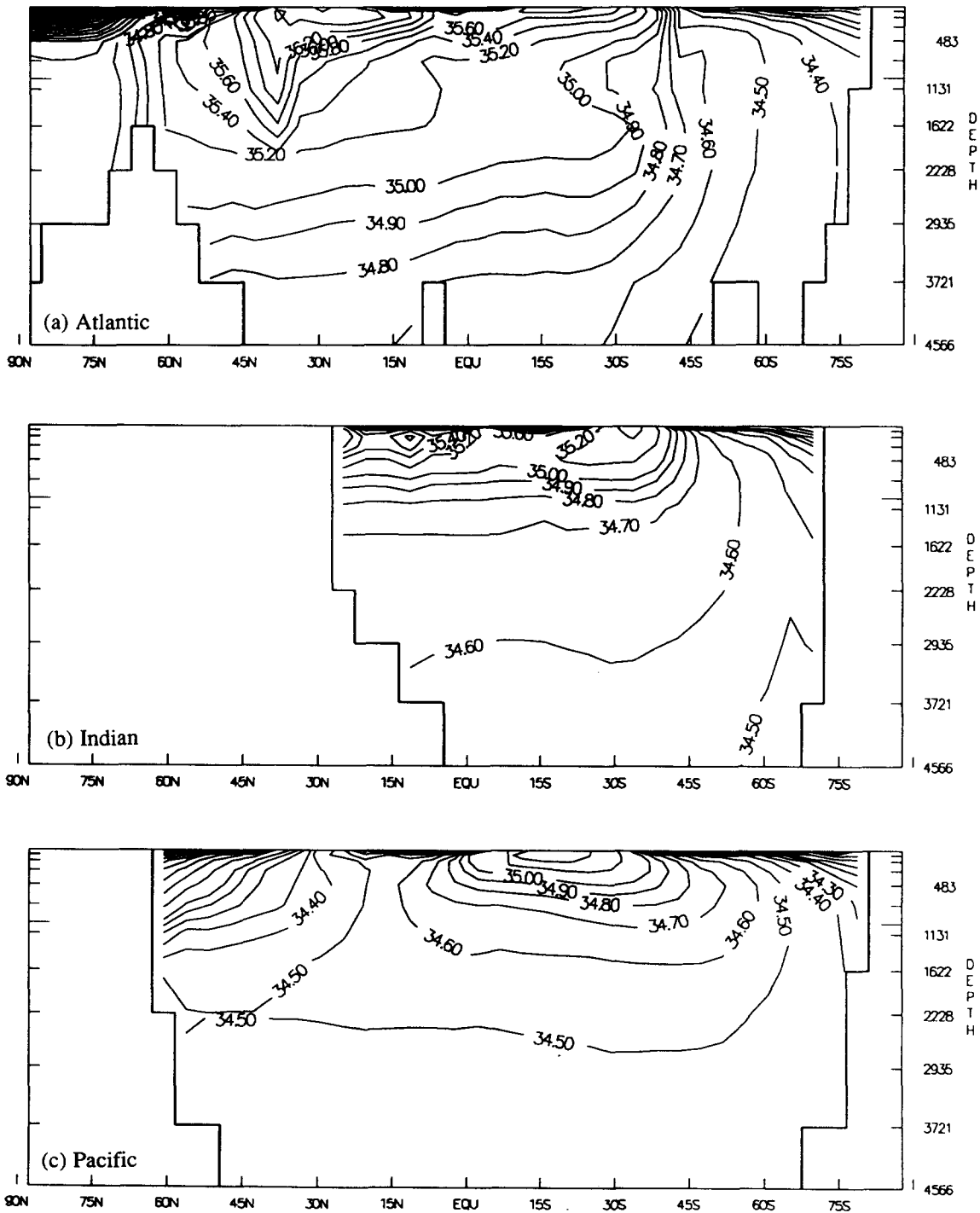


Fig. 12. Zonally-averaged salinity (parts per thousand) in the (a) Atlantic, (b) Indian and (c) Pacific basins of Expt. I. Contour interval is 0.2‰ except in the range 34.0‰–35.0‰, where the interval is 0.1‰.

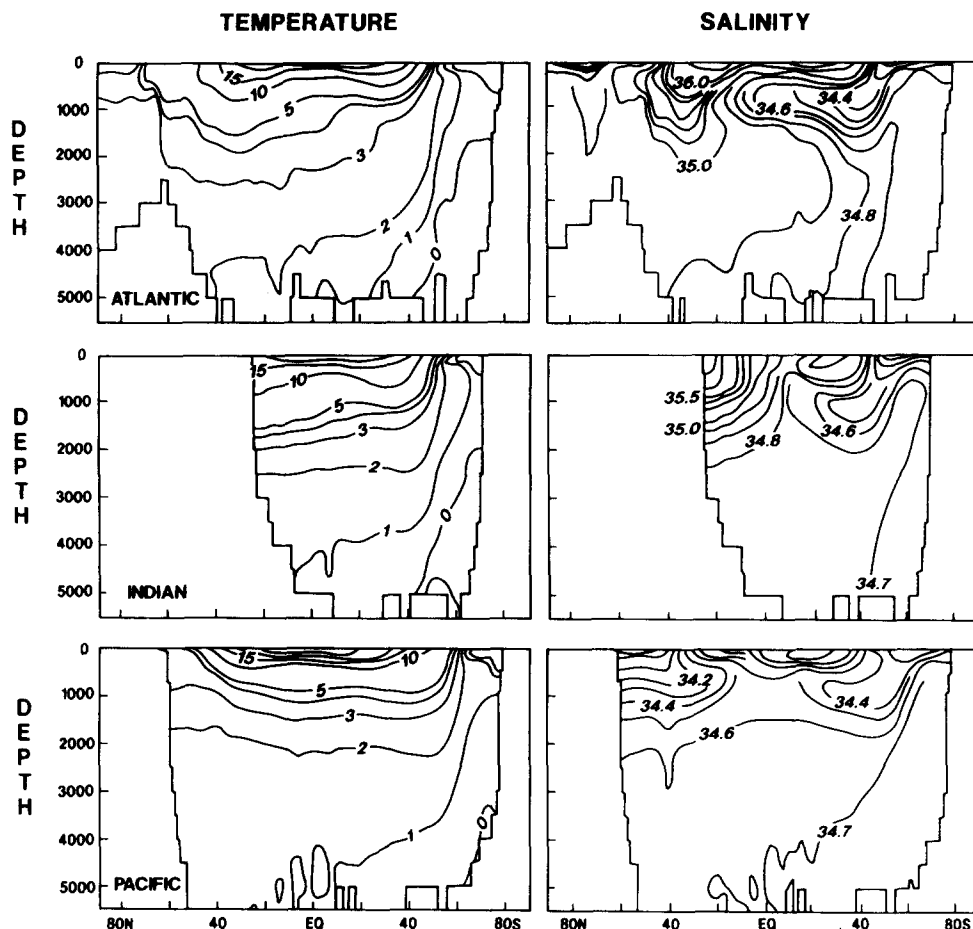


Fig. 13. Observed long-term mean basin-averaged potential temperature and salinity redrafted from Levitus (1982).

Sea (and to a lesser extent, Ross Sea), in agreement with observational data (Gill, 1973; Foster and Carmack, 1976; Foster and Middleton, 1980). However, it will be seen that the region of air-sea interaction matching the bottom water formation occurs at about 60°S, primarily because the near-surface water in the Weddell and Ross Seas remains far too fresh in the MS model.

As a final note in this discussion of meridional overturning and vertical motion in the MS model, it is important to remember the role of convective adjustment in forming deep water masses in the GFDL OGCM. Whenever the vertical stratification of the model ocean becomes unstable, temperature and salinity are mixed completely over the unstable portion of the water column. As such, the process of convection appears as a

source term in the tracer equations of the model. The vertical motion then only responds to the *effects* of convection, and not to the convective process itself. Consequently, convective adjustment can transport near surface water mass properties into the deep ocean, without necessarily producing a corresponding vertical motion. In the MS model, convective overturning of near surface water occurs in the extreme Southern Ocean of each experiment, and in the North Atlantic of Expt. I.

Water-mass distribution in the coupled model and climatology

The World's climate depends on the ocean-atmosphere heat and moisture balance, which is

inherently linked to the formation of water masses in the global ocean. It is therefore important that any model used to investigate climate change be

able to simulate the largest-scale features of water-mass formation. For example, Stouffer et al. (1989) use a heat and freshwater flux adjustment

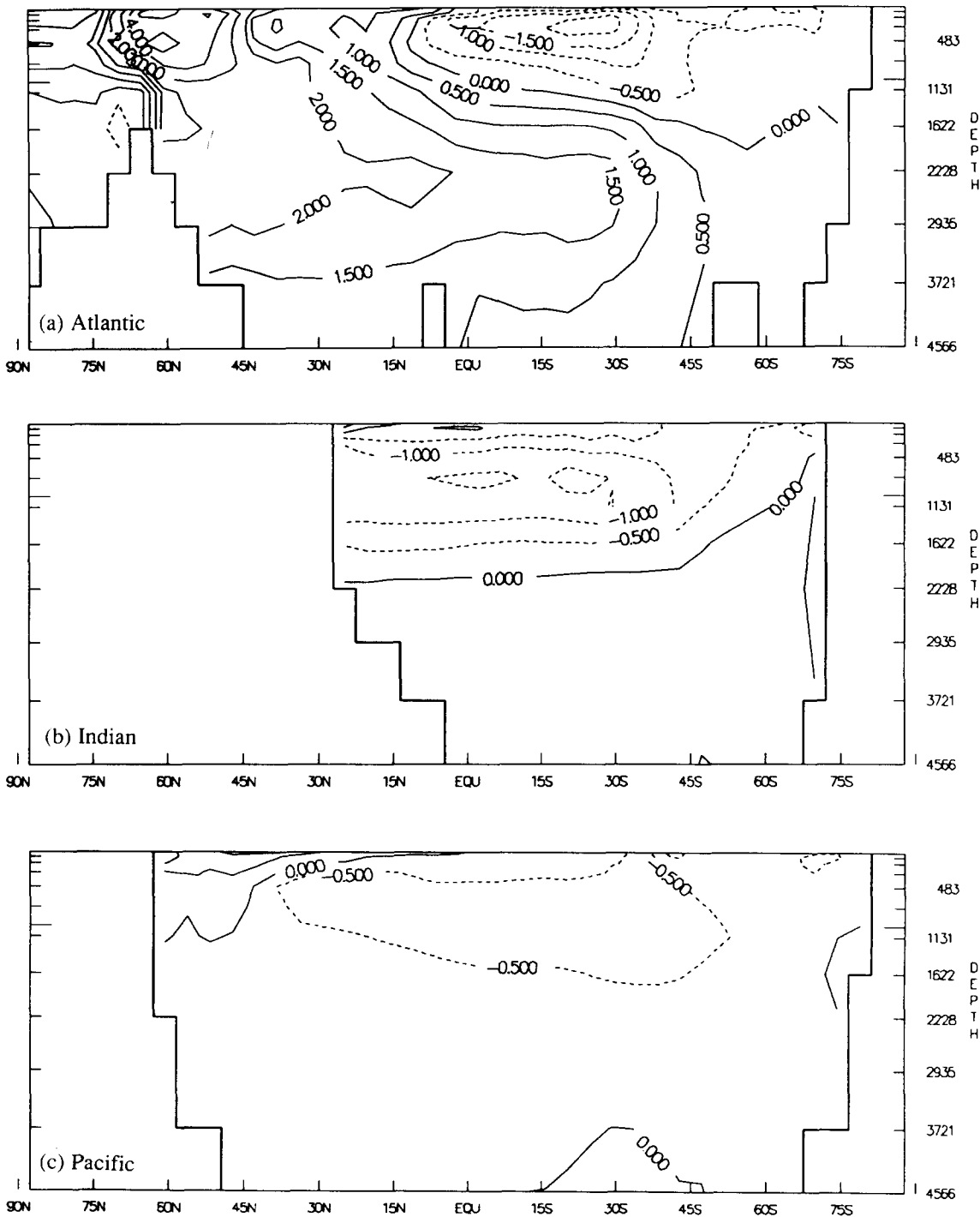


Fig. 14. Difference (Expt. I minus Expt. II) between the simulated basin-averaged potential temperature in each ocean basin. Contour interval is variable (either 0.5°C or 1°C) and chosen to highlight differences in the deep ocean.

in order to simulate NADW formation in a model used to study climate sensitivity to changes in atmospheric CO₂ concentrations.

It is useful to examine latitude–depth sections of the water mass properties in the MS model on a basin average domain. This will give an idea of

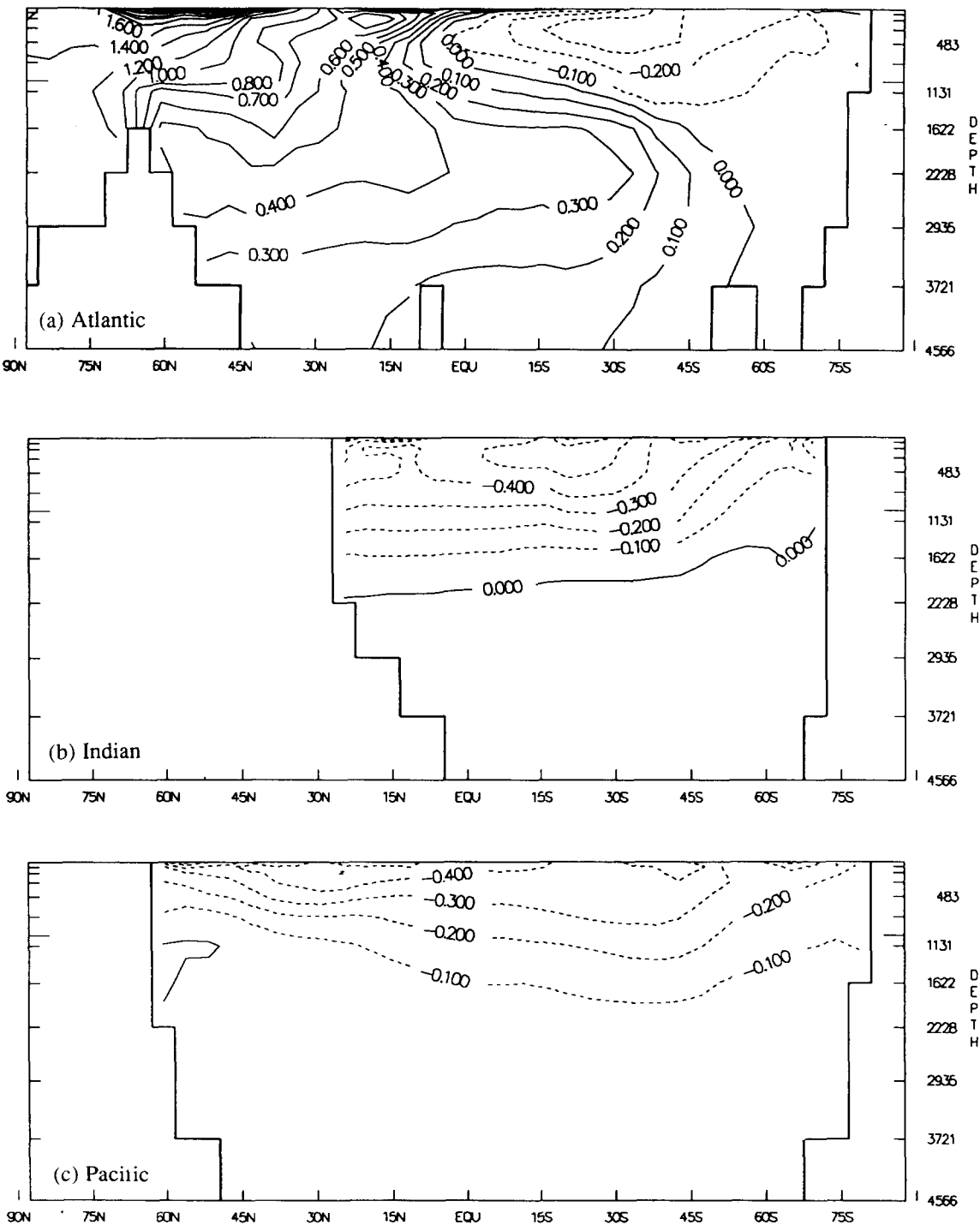


Fig. 15. Difference (Expt. I minus Expt. II) between the simulated basin-averaged salinity in each ocean basin. Contour interval is variable (either 0.1‰ or 0.2‰) and chosen to highlight differences in the deep ocean.

the ability of the model to reproduce the observed intermediate and deep water-mass characteristics. Figures 11 and 12 show the zonally-averaged potential temperature and salinity in the Atlantic, Indian and Pacific basins of Expt. I. To provide a climatological reference with which the MS simulation can be compared, the long-term mean basin-averaged temperature and salinity fields reported by Levitus (1982) are presented in Fig. 13. The comparison between modelled and observed water masses will focus on the simulation of Expt. I, since this mode more closely resembles the present day World climate. Nevertheless, as a comparison between the two experiments of MS, Figs. 14 and 15 show the difference between basin-averaged temperature and salinity simulated in Expts. I and II.

The large-scale *structure* of the temperature field in Expt. I appears to be in broad agreement with observations, even though the bottom water simulated is far too warm. In contrast, the structure of the salinity field is quite different to the climatological distributions shown in Fig. 13. In particular, there is no low salinity tongue of Antarctic Intermediate Water (AAIW) in the Southern Ocean of either experiment.

The sinking of NADW is apparent in the Atlantic section of Expt. I (Figs. 11a, 12a), where the deep temperature and salinity distributions are enhanced by the overturning of warm salty water in the region. However, the salinity section reveals that the NADW is probably not overturning with the intensity or depth it does in the real ocean. For example, in the climatological data, the basin-averaged 34.80 ‰ isohaline extends as far south as 30°S near the bottom of the ocean (at 4000 m depth). In comparison, the basin-averaged 34.80 ‰ isohaline *never* penetrates the 3721 m depth level in Expt. I, even in the far North Atlantic. This is because the deep North Atlantic ventilation is coming from the deep equatorial cell (Fig. 8a), rather than from the overturning of warm salty NADW. The equatorial cell ventilates the deep North Atlantic with relatively fresh water originating from the Southern Ocean.

The Southern Ocean salinity field is quite constant from basin to basin (Fig. 12) and as men-

tioned above, in sharp disagreement with observation. There is no low salinity tongue spreading equatorward at intermediate depths originating from the subtropical convergence zone. Furthermore, there is only weak formation of North Pacific Intermediate Water (NPIW). The lack of AAIW and NPIW formation was at first thought to be a result of insufficient vertical resolution at intermediate depths of the MS model. However, it turns out to be caused by the difference between climatological surface buoyancy fluxes and those that evolve at the surface of the MS coupled model. For example, using similar vertical resolution, England (1992) captures the major features of intermediate and deep water mass formation in an ocean GCM forced by an appropriately adjusted climatology at the sea surface. It turns out that the bottom water formed in the Weddell and Ross Seas needs to be sufficiently saline if the model is to capture Antarctic and North Pacific Intermediate Water formation.

In the extreme Southern Ocean of both experiments, there is an intense near-surface halocline in the immediate vicinity of Antarctica (Figs. 12 and 15), which prohibits deep water formation in the Weddell and Ross Seas. At deeper levels, however, the potential temperature and salinity are nearly uniform with depth, suggesting that intense convective overturning is drawing near-surface water into the deeper layers of the model. This occurs in the real ocean with the formation of Antarctic Bottom Water (AABW). However, the MS bottom water is characterised by a potential temperature of 3–4°C and a salinity of 34.40‰ in each ocean basin, whereas in reality AABW is significantly cooler and saltier (and hence much denser). The climatology of Levitus (1982) suggests that AABW has a temperature of 0–1°C and a salinity of about 34.73 ‰. This discrepancy between simulated and observed bottom water characteristics was at first thought to be a result of the extremely strong vertical motion associated with the so-called Deacon Cell (discussed in the previous section), which transports relatively warm and fresh mid-latitude water deep into the ocean interior at 35–50°S. However, it seems to be linked to the model having no seasonal insolation at the top of the atmosphere. By

having no seasonal insolation, the extreme Southern Ocean does not form as much ice as it does in reality during austral winter, and therefore surface salinities adjacent to Antarctica remain unrealistically fresh in the MS integrations. On top of this, there is no intensification of wind stress (and hence evaporation) characterising the winter season, so that again salinity remains too fresh in the Weddell and Ross Seas. Without the high salinity shelf water in the extreme Southern Ocean, the MS model allows surface water at 60°S to sink to the bottom, because it is denser (through its salinity) than the fresh Weddell Sea water. A recent integration of a coupled ocean–atmosphere model *with* seasonal insolation (Manabe et al., 1991) does not appear to correctly simulate the density of AABW on an annual average. This is probably a consequence of the freshwater flux adjustment term, which tends to restore the surface salinity field towards the seasonal climatology of Levitus (1986). This climatology is thought to be too fresh in the extreme Southern Ocean during winter.

Notice that the bottom water spreads further north in the Pacific and Indian basins than in the Atlantic sector in Expt. I, because there is little competition for forming the deep and bottom waters in these basins. Indeed, the salinity and temperature sections of the second Expt. (not shown) reveal that the AABW spreads well into the Northern Hemisphere of all three basins, because no deep water is formed in the North Atlantic.

The differenced sections of temperature and salinity (Figs. 14 and 15) reveal the significant thermohaline response of the World Ocean to the formation of NADW. In the Atlantic basin, NADW serves to enhance the warmth and salinity of the deep ocean, with an anomalous tongue of water appearing at about 2500 m depth. Earlier we noted a net transport of 8 Sv of NADW into the Southern Ocean (Fig. 8a). This is manifested in the extra heat and salt content of the deep Indian Ocean in Expt. I (Figs. 14b, 15b), indicating that NADW has been transported there via the ACC. However, the deep Pacific is both cooler and fresher almost everywhere in Expt. I, suggesting that the “thermohaline conveyor belt”

of Broecker et al. (1985) is not a component of the thermohaline circulation in Expt. I. In the Pacific and Indian Oceans, the near-surface differences in temperature and salinity are more a manifestation of differences in the atmospheric component of the MS experiments. For example, the warmer North Pacific in Expt. I is due to the zonal transport of warmer North Atlantic air temperatures through the model atmosphere.

Discussion

The description of circulation in the MS states was extended to include an analysis of the horizontal and meridional mass transport streamfunctions. The barotropic streamfunction was estimated by a Sverdrup model of depth-integrated flow that allows for circulation around islands. It was found that the broadest features of the MS barotropic mass transport are resolved by the Sverdrup model, except notably in the North Atlantic of Expt. I, where the circulation is driven by gradients in the thermohaline field as well as by surface wind stresses. It was also found that the Sverdrup model estimates a Pacific to Indian Ocean throughflow of about 16 Sv in the two runs. In the MS model, the mass transport through the Indonesian Passage vanishes, in sharp disagreement with the Sverdrup estimate. The closure of the Indonesian Passage to a barotropic throughflow serves to weaken the Agulhas Current by about 16 Sv, and strengthen the East Australian Current by the same amount. Recently, Hirst and Godfrey (1992) have shown that this results in a significant redistribution of heat in the Southern Hemisphere, particularly in the region of the Agulhas and East Australian Currents. In a comparison between a run with a non-zero net throughflow and one with only a baroclinic throughflow (i.e., similar to the MS ocean), the implied net surface heat flux varies by up to 60 W/m² over a substantial region of the Agulhas outflow. It is important, then, that this be considered when evaluating the MS-type model in climate research.

Basin-averaged temperature and salinity and the zonally-integrated meridional mass transport were used to describe the location and nature of water mass formation in the MS states. It was

found that the MS ocean does not form sufficiently dense bottom water adjacent to Antarctica. In fact, the bottom water in the modelled ocean originates from regions normally associated with Antarctic Intermediate Water formation (i.e., at about 60°S). Furthermore, the bottom water is characterised by a salinity of 34.40 ‰, and a temperature of 3–4°C, closely matching the water mass signature of AAIW. In the Weddell and Ross Seas, there is a sharp halocline prohibiting deep water formation adjacent to Antarctica. Salinity at the surface is less than 33.50 ‰, perhaps a result of the annual insolation of the model atmosphere. Without seasons, winter ice formation and enhanced evaporation are not simulated near the poles.

No intermediate water is formed in the MS model, primarily because there is no source of sufficiently dense bottom water close to Antarctica. Without this dense bottom water, the “would-be” intermediate water at 60°S sinks to great depths and actually becomes the model ocean’s bottom water. Whilst North Atlantic Deep Water is formed in the first experiment, its downward and southward penetration is somewhat weaker than in observation. It was shown that a deep overturning circulation centred just south of the equator brings fresh Southern Ocean water into the deep North Atlantic. These failures in reproducing the observed water mass structure of the World Ocean represent a shortcoming in the MS model, since the formation of water masses is inherently linked to the global budgets of heat and freshwater.

The coupled ocean–atmosphere model is a relatively new tool for climate research. It is particularly useful for studying the climate response to an imposed increase in the concentration of greenhouse gases in the atmosphere, since the ocean plays a vital role in determining the time scales of climate change. Many recent greenhouse studies have employed a coupled model much like that used by MS. It is clearly important that the coupled model be able to truly represent the climate system. Studies such as these investigate the quality of the numerical model without turning to an extensive integration of the equations of state and motion.

Acknowledgements

Ron Stouffer and Suki Manabe kindly provided data from the Manabe and Stouffer (1988) coupled ocean–atmosphere experiments. A thoughtful review of the original manuscript by Andrew Weaver is also acknowledged.

References

- Brewer, P.G., Broecker, W.S., Jenkins, W.J., Rhines, P.B., Swift, J.H., Takahashi, T. and Williams, R.T., 1983. A climatic freshening of the deep Atlantic north of 50°N over the past 20 years. *Science*, 222: 1237–1239.
- Broecker, W.S., Peteet, D.M. and Rind, D., 1985. Does the ocean–atmosphere system have more than one stable mode of operation? *Nature*, 315: 21–26.
- Bryan, F., 1986. High latitude salinity effects and interhemispheric thermohaline circulations. *Nature*, 323: 301–304.
- Bryan, K., 1969. A numerical method for the study of the circulation of the World Ocean. *J. Comput. Phys.*, 3: 347–376.
- Bryan, K., 1984. Accelerating the convergence to equilibrium of ocean–climate models. *J. Phys. Oceanogr.*, 14: 666–673.
- Bryan, K. and Lewis, L.J., 1979. A water mass model of the World Ocean. *J. Geophys. Res.*, 85(C5): 2503–2517.
- Bryan, K. and Spelman, M.J., 1985. The ocean’s response to a carbon dioxide-induced warming. *J. Geophys. Res.*, 90(C6): 11, 679–11, 688.
- Bryan, K., Manabe, S. and Spelman, M.J., 1988. Interhemispheric asymmetry in the transient response of a coupled ocean–atmosphere model to a CO₂ forcing. *J. Phys. Oceanogr.*, 18: 851–867.
- Bryan, K., Komro, F.G., Manabe, S. and Spelman, M.J., 1982. Transient response to increasing atmospheric carbon dioxide. *Science*, 215: 56–58.
- Chelton, D.B., Mestas-Nunez, A.M. and Freilich, M.H., 1990. Global wind stress, wind stress curl and Sverdrup circulation from the Seasat Scatterometer. *J. Phys. Oceanogr.*, 20: 1175–1250.
- Cox, M.D., 1984. A primitive equation, three-dimensional model of the ocean. GFDL Ocean Group Tech. Rep. No. 1, 143 pp.
- de Szoeke, R.A., 1987. On the wind-driven circulation of the South Pacific Ocean. *J. Phys. Oceanogr.*, 17: 613–630.
- Deacon, G.E.R., 1937. Note on the dynamics of the Southern Ocean. *Discovery Rep.*, Cambridge University Press, 15: 125–152.
- England, M.H., 1991. An analysis of the dynamics and circulation in a global coupled ocean–atmosphere model. *Ocean Sci. Inst. Rep. No. 44*, Univ. of Sydney, 111 pp.
- England, M.H., 1992. On the formation of Antarctic Intermediate and Bottom Water in ocean general circulation models. *J. Phys. Oceanogr.* (in press).

- Evenson, A.J. and Veronis, G., 1975. Continuous representation of wind stress curl over the world ocean. *J. Mar. Res.*, 33 (Supplement): 131–144.
- Folland, C.K., Palmer, T.N. and Parker, D.E., 1986. Sahel rainfall and worldwide sea temperatures, 1901–85. *Nature*, 320: 602–607.
- Foster, T.D. and Carmack, E.C., 1976. Frontal zone mixing and Antarctic bottom water formation in the southern Weddell Sea. *Deep-Sea Res.*, 23: 301–317.
- Foster, T.D. and Middleton, J.H., 1980. Bottom water formation in the western Weddell Sea. *Deep-Sea Res.*, 27: 367–381.
- Gill, A.E., 1973. Circulation and bottom water formation in the Weddell Sea. *Deep-Sea Res.*, 20: 111–140.
- Gill, A.E. and Schumann, E.H., 1979. Topographically induced changes in the structure of an inertial coastal jet: application to the Agulhas Current. *J. Phys. Oceanogr.*, 9: 975–991.
- Godfrey, J.S., 1989. A Sverdrup model of the depth-integrated flow for the World Ocean allowing for island circulations. *Geophys. Astrophys. Fluid Dynamics*, 45: 89–112.
- Hellerman, S. and Rosenstein, M., 1983. Normal monthly wind stress over the World Ocean with error estimates. *J. Phys. Oceanogr.*, 13: 1093–1104.
- Hirst, A.C. and Godfrey, J.S., 1992. The role of the Indonesian throughflow in a global ocean GCM. *J. Phys. Oceanogr.*, (in press).
- Hsieh, W.W. and Gill, A.E., 1984. The Rossby adjustment problem in a rotating, stratified channel, with and without topography. *J. Phys. Oceanogr.*, 14: 424–437.
- Jones, P.D., Wigley, T.M.L. and Wright, P.B., 1986. Global temperature variations between 1861 and 1984. *Nature*, 322: 430–434.
- Killworth, P.D., 1987. Topographic instabilities in level model OGCM's. *Ocean Modelling*, 75: 9–12.
- Levitus, S., 1982. Climatological atlas of the World Ocean. NOAA Prof. Paper 13, U.S. Dept. Commerce, Washington, DC, 173 pp.
- Levitus, S., 1986. Annual cycle of salinity and salt storage in the World Ocean. *J. Phys. Oceanogr.*, 16: 322–343.
- Luyten, J., Pedlosky, J. and Stommel, H., 1983. The ventilated thermocline. *J. Phys. Oceanogr.*, 13: 292–309.
- Maier-Reimer, E. and Mikolajewicz U., 1989. Experiments with an OGCM on the cause of the Younger Dryas. Report No. 39, Max-Planck-Institut für Meteorologie, Hamburg. Reprinted from: *Oceanography 1988* (Eds. A. Ayala-Castanares, W. Wooster and A. Yanez-Arancibia), UNAM Press, Mexico D.F., pp. 87–100.
- Manabe, S. and Bryan, K., 1969. Climate calculations with a combined ocean-atmosphere model. *J. Atmos. Sci.*, 26: 786–789.
- Manabe, S. and Bryan, K., 1985. CO₂-induced change in a coupled ocean-atmosphere model and its implications. *J. Geophys. Res.*, 90(C11): 11, 689–11, 707.
- Manabe, S. and Stouffer, R.J., 1988. Two stable climates in a coupled ocean-atmosphere model. *J. Climate*, 1: 841–866.
- Manabe, S., Bryan, K. and Spelman, M.J., 1990. Transient response of a global ocean-atmosphere model to a doubling of atmospheric carbon dioxide. *J. Phys. Oceanogr.*, 20: 722–749.
- Manabe, S., Stouffer, R.J., Spelman, M.J. and Bryan, K., 1991. Transient responses of a coupled ocean-atmosphere model to gradual changes of atmospheric carbon dioxide. Part I: Annual mean response. *J. Climate*, 4: 785–818.
- Marotzke, J. and Willebrand, J., 1991. Multiple equilibria of the global thermohaline circulation. *J. Phys. Oceanogr.*, 21: 1372–1385.
- Marotzke, J., Welander, P. and Willebrand, J., 1988. Instability and multiple steady states in a meridional-plane model of the thermohaline circulation. *Tellus*, 40A: 162–172.
- Roemmich, D. and Wunsch, C., 1984. Apparent changes in the climatic state of the deep North Atlantic Ocean. *Nature*, 307: 447–450.
- Semtner, A.J. and Chervin, R.C., 1988. A simulation of the global ocean circulation with resolved eddies. *J. Geophys. Res.*, 93: 15, 502–15, 522.
- Sprintall, J. and Tomczak, M., 1991. On the formation of Central Water and thermocline ventilation in the Southern Hemisphere. *Deep Sea Res.* (in press).
- Stouffer, R.J., Manabe, S. and Bryan, K., 1989. Interhemispheric asymmetry in climate response to a gradual increase of atmospheric CO₂. *Nature*, 342: 660–662.
- Street-Perrott, F.A. and Perrott, R.A., 1990. Abrupt climate fluctuations in the tropics: the influence of Atlantic Ocean circulation. *Nature*, 343: 607–612.
- Toggweiler, J.R., Dixon, K. and Bryan, K., 1989a. Simulations of radiocarbon in a coarse-resolution world ocean model. I: Steady state prebomb distributions. *J. Geophys. Res.*, 94: 8217–8242.
- Toggweiler, J.R., Dixon, K. and Bryan, K., 1989b. Simulations of radiocarbon in a coarse-resolution world ocean model. II: Distributions of bomb-produced Carbon 14. *J. Geophys. Res.*, 94: 8243–8264.
- Washington, W.M. and Meehl, G.A., 1989. Climate sensitivity due to increased CO₂: experiments with a coupled atmosphere and ocean general circulation model. *Clim. Dynamics*, 4(1): 1–38.
- Weaver, A.J. and Sarachik, E.S., 1991. The role of mixed boundary conditions in numerical models of the ocean's climate. *J. Phys. Oceanogr.*, 21: 1470–1493.
- Weaver, A.J., Sarachik, E.S. and Marotzke, J., 1991. Freshwater flux forcing of decadal and interdecadal oceanic variability. *Nature*, 353: 836–838.
- Welander, P., 1959. On the vertically integrated mass transport in the oceans. In: B. Bolin (Editor), *The Atmosphere and the Sea in Motion*. Rockefeller Inst. Press and Oxford Univ. Press, pp. 95–101.
- Welander, P., 1986. Thermohaline effects in the ocean circulation and related simple models. In: J. Willebrand and D.L.T. Anderson (Editors), *Large-Scale Transport Processes in the Oceans and Atmosphere*. D. Reidel, Dordrecht, pp. 163–200.